Ligand Non-innocence in Nickel Porphyrins: Nickel Isobacteriochlorin Formation Under Hydrogen Evolution Conditions

Andrew G. Maher, Mengran Liu and Daniel G. Nocera*

Department of Chemistry and Chemical Biology, Harvard University, 12 Oxford Street, Cambridge, Massachusetts 02138, United States

Supporting Information Placeholder

ABSTRACT: An electron-deficient nickel porphyrin complex undergoes facile ring-reduction to form a nickel isobacteriochlorin complex under hydrogen evolution conditions. Spectroscopic experiments indicate that the reduced nickel porphyrin undergoes subsequent reduction and protonation to form a phlorin anion rather than a metal-hydride, demonstrating that the key initial proton-coupled electron transfer step is directed toward the ligand versus the metal. The phlorin anion facilely converts to the isobacteriochlorin in the presence of two-electron and three-proton equivalents. Cyclic voltammetry (CV) and spectroscopic experiments reveal that the 4-electron, 4-proton electrochemical reduction of nickel porphyrin to isobacteriochlorin occurs promptly in the presence of the strong proton donor, tosic acid, followed by hydrogen evolution reaction (HER) catalysis at slightly more negative potentials. CVs of independently synthesized Ni isobacteriochlorin show catalytic HER at the same potentials as that observed for HER in CVs of the Ni porphyrin. We find that under strongly acidic conditions, the HER catalysis arises from conversion of the Ni isobacteriochlorin into a nickel-containing, catalytically active electrode-adsorbed species. These results show that Ni porphyrin converts to Ni isobacteriochlorin under HER catalysis conditions via a ligand-based PCET process, and that it is the reduced isobacteriochlorin complex that gives rise to an active HER catalysis.

Introduction

The electrochemical generation of chemical fuels as a means of storing solar energy is a viable strategy to address an increasing global energy demand in a renewable and carbon-neutral manner.[1–3] The formation of even the most basic of these fuels, H_2, requires a catalysis derived from multi-electron, multi-proton reactions. Such processes require the coupling of electrons to protons in order to avoid high-energy intermediates that impose kinetic and thermodynamic barriers to efficient catalysis.[4–8] Well-designed molecular catalysts facilitate proton-coupled electron transfer (PCET) as a result of finely-tuned control of structural and electronic properties. In the last decade, a number of hydrogen evolution reaction (HER) catalysts containing earth-abundant transition metals have been elaborated.[9–16] The HER catalysts that successfully exploit PCET processes typically do so by promoting protonation and redox events that occur at the active metal center (the $L_nM(e^-,H^+)$ PCET motif, Chart 1), often via the installation of proton relays in the secondary coordination sphere.[12, 17 – 23] However, greater appreciation for an alternative PCET motif has emerged in recent years: one in which a metal-centered electron transfer is ultimately coupled to the protonation of the ligand itself,[14, 24 – 28] an "$L_n(H^+)M(e^-)$" process (Chart 1). Internal electron transfer or strong coupling between metal-based and ligand-based orbitals are likely necessary for such processes to occur.

Ligand non-innocence has been invoked for HER catalysis promoted by metalloporphyrins of first row transition metals.[29, 30] The propensity of the porphyrin macrocycle to accept multiple electron and proton equivalents engenders ambiguity as to the site of reactivity during catalysis and raises the possibility of $L_n(H^+)M(e^-)$-type PCET processes playing a key role. Accordingly, a deeper understanding of ligand non-innocence in PCET activation of small molecules by porphyrin macrocycles is an ideal venue in which to explore the $L_n(H^+)M(e^-)$-type motif.

Chart 1. Metal-only and metal-ligand PCET motif.

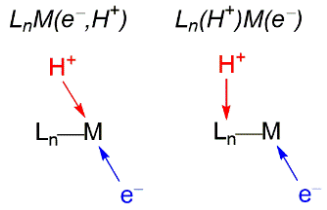

Computed HER pathways of the electron-poor nickel porphyrin **Ni-P** (Chart 2) have led to a proposed mechanism involving the protonation of the *meso* carbon occurring after a single one-electron reduction in the case of strong proton donors or after two one-electron reductions in the case of weaker proton donors;[30] a common intermediate in both the strong acid and weak acid computed HER cycles is proposed to be the Ni phlorin anion species [**Ni-Phl**]$^-$ (Chart 2). In this case, hydrogen generation is predicted without the need for the direct protonation of the metal center, in contradistinction to other reports of HER catalysis by **Ni-P** that invoke metal-centred $L_nM(e^-,H^+)$ reactivity involving metal-hydride intermediates.[31] Although the phlorin-based mechanism proposes unconventional reactivity, calculations suggest the phlorin to be more accessible thermodynamically than the more commonly invoked metal-hydride.

Chart 2. Ni porphyrin **Ni-P**, Ni phlorin anion [**Ni-Phl**]$^-$, and Ni isobacteriochlorin **Ni-iBC**.

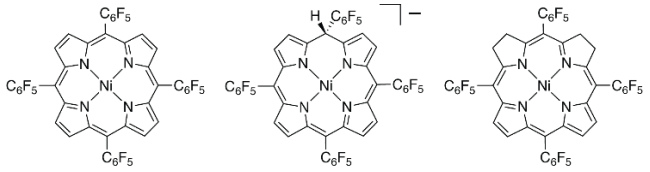

With a growing cognizance of ligand non-innocence emerging, understanding the site of protonation is warranted in proposed HER mechanisms, especially those involving catalysts comprising macrocycles with extended conjugated and/or aromatic rings. Phlorin formation is typically cited as an initial step of porphyrin ring reduction with subsequent formation of hydroporphyrins such as chlorins (hydrogenation of one C_β-C_β bond), bacteriochlorins (hydrogenation of two opposite C_β-C_β bonds), and isobacteriochlorins (hydrogenation of two adjacent C_β-C_β bonds) upon additional protonations, reducing equivalents, and prototropic tautomerizations.[32–37] Consequently, an intriguing issue is the role of the reduced hydroporphyrin complexes in HER. Along these lines, a report of photosensitized H_2 generation from Zn porphyrins posits an *in situ*-formed Zn chlorin species as the intermediate responsible for hydrogen formation.[38] Similarly, enhanced HER activity for nickel hydroporphyrins has been reported versus nickel porphyrin.[39] Other recent reports have demonstrated electrocatalytic activity from zinc bacteriochlorins [40] and other hydroporphyrinoids. [41] However, the propensity for ligand-hydrogenation to lead to the conversion of molecular complexes and the formation of catalytically active heterogeneous films or nanoparticles, as has been reported for a number of Co[42–44] and Ni[45–47] complexes in recent years, underscores the necessity of a comprehensive mechanistic investigation of molecular catalysts that are prone to ligand-based reduction.

We report herein a unified mechanistic description of Ni porphyrin ↔ hydroporphyrin interconversion under the reducing and protic conditions of HER. **Ni-P** converts to nickel phlorin anion [**Ni-Phl**]$^-$, which leads to the *in situ*-generation of Ni isobacteriochlorin **Ni-iBC**. Formation of a nickel-containing surface-adsorbed active HER catalytic species is observed during electrochemical reduction of **Ni-iBC** under strongly protic conditions, indicating that **Ni-iBC** serves as a precursor for HER.

Experimental

Materials. All manipulations and sample preparations were performed in an N_2-atmosphere glovebox, unless otherwise noted. ^{1}H NMR spectra (500 MHz) were recorded on samples at room temperature. Neutral alumina was dried under vacuum while being heated to 140 °C. Solvents CH_3CN, CH_2Cl_2, and toluene were dried with a Glass Contour Solvent Purification System manufactured by Pure Process Technology, by passing through an activated column under argon. Tetra-*n*-butylammonium hexafluorophosphate ($TBAPF_6$, ≥99.0% purity) was recrystallized in ethanol and dried under vacuum. 5,10,15-tetra(pentafluorophenyl)porphine was purchased from Frontier Scientific. *p*-Toluenesulfonic acid (tosic acid), benzoic acid, phenol, trifluoroacetic acid, dimethyl-*p*-toluidine, cobaltocene, and decamethylcobaltocene were all purchased from Sigma Aldrich and used as received.

Ni-P and Zn-P. The free base 5,10,15,20-tetra(pentafluorophenyl)porphine was metalated with $Ni(OAc)_2$ or $Zn(OAc)_2$ and subsequently purified by silica gel column chromatography, as previously reported. [18,54]

[**Ni-Phl**]$^-$. An excess of sodium mercury amalgam (5%) was added to a solution of **Ni-P** (5.2 mg, 5×10^{-6} mol) in 5 mL of toluene. The solution was then stirred for 3 h. During the reaction, the color of the solution changed from dark red to dark brown/yellow, and the UV-vis absorption spectrum taken after 3 h in CH_3CN is shown in Figure S1. The reaction mixture was removed from the sodium amalgam and dried *in vacuo*. ^{1}H NMR: δ/ppm (CD_3CN): 7.12 (d, J = 5.0 Hz, 2H), 6.88 (d, J = 5.0 Hz, 2H), 6.86 (d, J = 5.0 Hz, 2H), 6.50 (d, J = 3.2 Hz, 2H), 5.25 (br s, 1H). HR-MS obsd. 1030.9874 (M^-); calcd. 1030.9867 (M = $C_{44}H_9F_{20}N_4Ni$). Alternatively, [**Ni-Phl**]$^-$ was prepared by bulk electrolysis of **Ni-P** in CH_3CN (0.1 M $TBAPF_6$) in a carbon crucible working electrode (Pt wire counter electrode) by applying a potential of −1.9 V vs. the ferrocenium/ferrocene (Fc^+/Fc) in the presence of 1.5 equiv of phenol. We include no elemental analysis for this or any other complex because the technique is inadequate for assessing the purity of large macrocycles. Due to the large number of light atoms (C, N, H) in the macrocyclic framework, small variations in the composition of the molecule (dehydration, protonation, etc.) are not detected by elemental analysis. As a result, this method provides little insight into the purity or identity of the molecule.

Ni-iBC. An excess of cobaltocene was first added to a solution of **Ni-P** (3.6 mg, 3.5×10^{-6} mol) in 5 mL of anhydrous CH_3CN. Then 0.4 mL of a 0.1 M stock solution of tosic acid (6.9 mg, 4×10^{-5} mol) in CH_3CN was added in small aliquots to the reaction mixture until the UV-vis absorption spectrum converted completely to that of **Ni-iBC**. The reaction mixture was then dried *in vacuo* and re-dissolved in 2 mL of CH_2Cl_2 (a solvent in which tosic acid has low solubility). The supernatant was then filtered through a short column of dried neutral alumina with a CH_2Cl_2/cyclohexane eluent and again dried *in vacuo*. ^{1}H NMR: δ/ppm ($CDCl_3$): 7.55 (d, J = 4.6 Hz, 2H), 7.12 (d, J = 4.6 Hz, 2H), 3.35 (s, 8H). HR-LCMS obsd. 1035.0073 ($M+H^+$); calcd. 1035.0169 (M = $C_{44}H_{12}F_{20}N_4Ni$).

Methods. UV-vis absorption spectra were recorded at room temperature in quartz cuvettes in anhydrous CH_3CN on either an Ocean Optics USB4000 spectrometer (coupled to a DT-mini-2-GS light source) or a Varian Cary 5000 UV-vis-NIR spectrophotometer.

X-ray photoelectron spectroscopy from a Thermo Scientific K-alpha XPS system was utilized to determine surface chemical composition of the electrolyzed glassy carbon plate. The sample was illuminated using a monochromated Al Kα X-ray source (1486.6 eV energy and 0.85 eV line width) 114 with a 400 μm spot size. Surface charging was compensated by a low energy (0–14 eV) electron flood gun. The system was precalibrated with Au, Ag, and Cu standards built into the sample stage using an automated routine. High-resolution spectra for P 2p, S 2p, C 1s, N 1s, O 1s, F 1s, Ni 2p, and Na 1s were measured with a step size of 0.1 eV. All spectra were then calibrated to the C 1s peak at 284.8 eV.

Electrochemical measurements were performed in a nitrogen-atmosphere glovebox at 295 K on a CH Instruments 760D

Electrochemical Workstation using CHI Version 10.03 software. Cyclic voltammetry experiments were performed in acetonitrile with 0.1 M $TBAPF_6$ as the supporting electrolyte. The working electrode was a glassy carbon button (3 mm diameter), the counter electrode was platinum wire, and the reference electrode was a non-aqueous Ag/Ag^+ apparatus from BioAnalytical Systems. All CVs were recorded with compensation for ohmic drop and were referenced to the ferrocenium/ferrocene (Fc^+/Fc) couple via the presence of a small amount of ferrocene in the sample solution. The solutions were stirred and the working electrode polished between each CV acquisition. A typical CV solution was 2.0 mL in volume, and acid was added via the addition of small aliquots of concentrated acid solution in order to minimize dilution.

Calculation of the working curves in the "trumpet" plot used to determine the standard heterogeneous rate constant for electron transfer, k_S^{ap}, was performed by simulating cyclic voltammograms using DigiElch 7 software.[48] Cyclic voltammograms (CVs) of a reversible reduction using the fixed parameters $a = 0.5$, $E^0 = 0.0$ V, $D = 7 \times 10^{-6}$ cm^2 s^{-1}, and $k_S = 0.1$ cm s^{-1} were simulated for a large range of scan rates. The working curves were generated by recording the cathodic and anodic peak potentials of each simulated CV as a function of scan rate. Via an iterative process the working curves were shifted until they agreed well with the experimental values, with the best fit allowing for the calculation of the experimental k_s^{ap}.

Thin-layer spectroelectrochemistry experiments were recorded in the glovebox with the Ocean Optics spectrometer using a 0.5 mm path length quartz cell, a platinum mesh working electrode, a platinum wire counter electrode, and a non-aqueous Ag/Ag^+ reference electrode, all of which were purchased from BioAnalytical Systems.

Controlled-potential bulk electrolysis experiments for H_2 detection were performed in a gas-tight glass electrochemical cell using a glassy carbon rod (7 mm × 5 cm) working electrode, platinum wire counter electrode, and Ag/Ag^+ reference electrode. Gas chromatography (GC) measurements were taken to quantify evolved H_2 gas, and the faradaic efficiency was determined using a calibration curve derived from H_2 gas standards generated by adding HCl to a known quantity of lithium triethylborohydride (a method previously validated by comparison with Toepler pump combustion experiments).[49] The bulk electrolysis of **Ni-iBC** in CH_3CN was performed by applying potential of ca. −1.6 V vs. Fc^+/Fc in the presence of 30 mM tosic acid. The headspace of the electrochemical cell was sampled, and quantitation yielded a faradaic efficiency of 86%.

Results

Formation, Characterization, and Reactivity of [Ni-Phl]⁻. DFT and spectroelectrochemical studies indicate that weak acids will protonate the doubly-reduced Ni porphyrin dianion **[Ni-P]²⁻** to generate a stable intermediate, whereas the use of acids of sufficient strength to protonate the monoanion **[Ni-P]⁻** will lead to further reduction and protonation.[30] Guided by these DFT predictions, our study to investigate the site of protonation of **Ni-P** initially focused on the second reduction process in the presence of weak acids, with the goal of identifying the initial product of a single protonation step. Toward this end, **[Ni-P]²⁻** was generated *in situ* via the gradual addition of decamethylcobaltocene (E^0 = −1.91 vs. Fc^+/Fc)[50] to a solution of **Ni-P** in CH_3CN. The progress of the reduction was monitored by UV-vis absorption (Figure 1a). With reduction, the Soret (399 nm) and Q bands

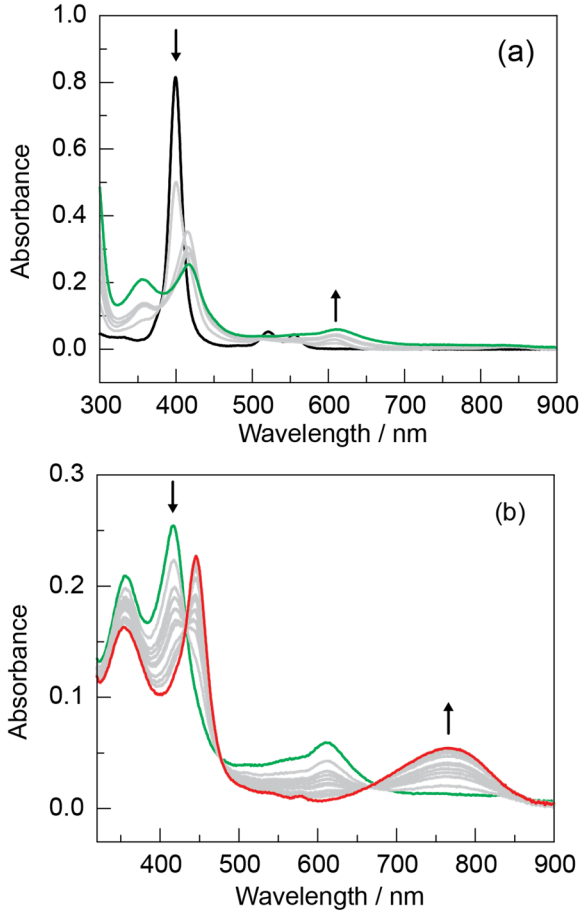

Fig. 1 (a) UV-vis absorption spectra showing the conversion of **Ni-P⁰** (—) to **[Ni-P]²⁻** (—) upon increasing concentrations of decamethylcobaltocene in CH_3CN. (b) UV-vis absorption spectra showing the conversion of the *in situ*-generated **[Ni-P]²⁻** (—) to **[Ni-Phl]⁻** (—) upon the addition of 1 equiv of phenol.

(520 nm and 555 nm) of **Ni-P⁰** decrease in intensity and new bands at 350 nm, 415 nm and 612 nm appear. A single set of isosbestic points are not observed in Figure 1a due to the formation of the monoanion **[Ni-P]⁻** at intermediate concentrations of reductant. The final spectrum (green line, Figure 1a) matches that of the **[Ni-P]²⁻** dianion produced using thin-layer spectroelectrochemistry,[30] with the exception of the peak observed at 350 nm, which corresponds to the decamethylcobaltocene present in solution. The addition of 1.0 equiv of the weak proton donor phenol (PhOH, pK_a = 29.1 in CH_3CN)[51] is accompanied by the disappearance of the bands at 415 nm and 612 nm and the appearance of a sharp absorption band at 445 nm and a very broad band centred at 765 nm, as shown in Figure 1b (the decamethylcobaltocene peak at 350 nm remains). These absorption features are consistent with those of phlorin anions,[33,34,52,53] and the overall spectrum matches that reported for the spectroelectrochemical reduction of **Ni-P** in the presence of PhOH.[30] Thus the species giving rise the final absorption profile shown in Figure 1b is assigned as **[Ni-Phl]⁻**. A species with an identical UV-vis absorption spectrum (Figure S1) was also generated by sodium/mercury amalgam reduction in toluene and by bulk electrolysis in CH_3CN (0.1 M $TBAPF_6$) at a potential of −1.9 V vs. Fc^+/Fc in

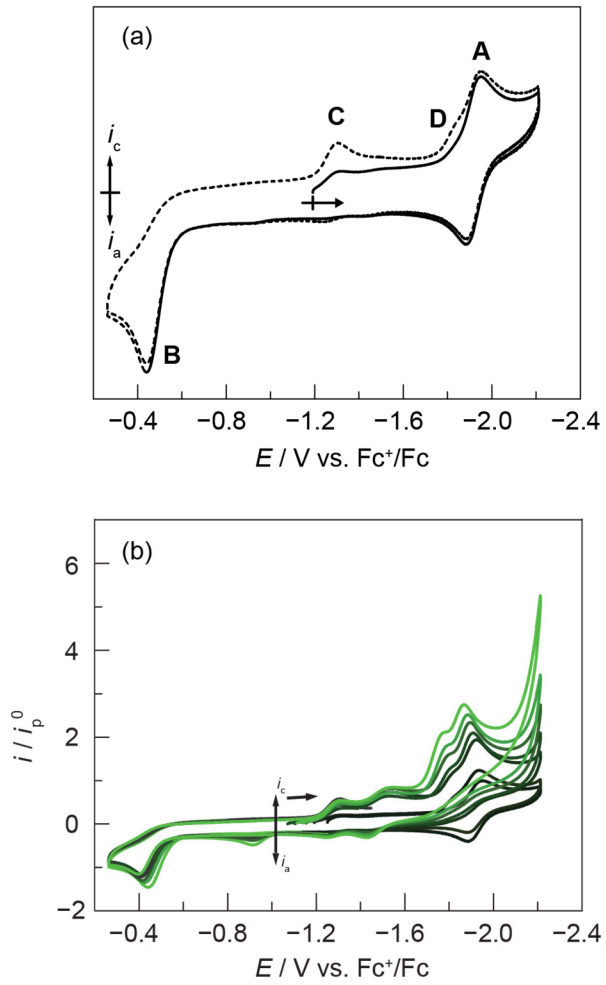

Fig. 2 (a) CV of [**Ni-Phl**]$^-$ (generated by bulk electrolysis) in CH_3CN (0.1 M $TBAPF_6$) at a scan rate of 0.1 V s^{-1}. Solid line: first scan; dashed line: second scan. (b) CVs of [**Ni-Phl**]$^-$ in the presence of 0 (—), 0.125, 0.25, 0.50, 1.0, 2.0 and 5.0 (—) mM benzoic acid. The current is normalized by the peak current observed in the absence of benzoic acid (i_p^0).

the presence of 1.5 equiv of phenol. Proton NMR (Figure S2) and high-resolution mass spectrometry (Figure S3) of the species isolated from the Na/Hg reduction in toluene are also consistent with the assignment of [**Ni-Phl**]$^-$.

The cyclic voltammogram (CV) of [**Ni-Phl**]$^-$ is presented in Figure 2a. Scanning initially in the cathodic direction, a single reversible wave centered at −1.92 V vs. Fc^+/Fc (wave **A**) is observed, as well as an irreversible oxidation wave with a peak potential of −0.44 V (wave **B**). A much smaller wave near the −1.27 V vs. Fc^+/Fc standard potential of the **Ni-P**$^{0/-}$ couple[54] is also observed, indicating the presence of a residual amount of **Ni-P** in the solution. When the CV is reversed in the cathodic direction following the irreversible oxidation process (dotted line, Figure 2a), a significant increase in current at the **Ni-P**$^{0/-}$ couple at −1.27 V is observed (wave **C**), along with the appearance of a wave on the shoulder of the **Ni-P**$^{-/2-}$ couple at −1.83 V (wave **D**). These results suggest that **Ni-P** is formed upon oxidation of [**Ni-Phl**]$^-$.

CVs of [**Ni-Phl**]$^-$ taken with increasing concentrations of benzoic acid (pK_a = 20.7 in CH_3CN)[55] are shown in Figure 2b. With benzoic acid present, there is again increased current at the **Ni-P**$^{0/-}$ couple, as well as a new reversible wave at approximately −1.47 V, though the currents of these CV features do not grow significantly as increasing amounts of benzoic acid are introduced. The wave at −1.92 V corresponding to the reduction of [**Ni-Phl**]$^-$ loses reversibility and increases in current as more benzoic acid is added. The peak potential of this reductive process, as well as that of the irreversible oxidative process near −0.44 V, both shift anodically upon the addition of benzoic acid. In Figure 2b, the ratio of the observed current to that of the one-electron wave in the absence of acid, i_p^0, does not exceed 3 at the −1.92 V process, even in the presence of a large excess of benzoic acid. The process is therefore not catalytic and is inconsistent with HER production by [**Ni-Phl**]$^-$ under these conditions of higher macrocyclic concentration as used here. Rather, it is suggestive of the formation of new product(s) formed from the protic reduction of [**Ni-Phl**]$^-$. The reversible wave at approximately −1.47 V in Figure 2b can be assigned to the ring-reduced species Ni isobacteriochlorin (**Ni-iBC**) formed during a disproportionation reaction that also produces an equivalent of **Ni-P** (*vide infra*), while the anodic peak at approximately −0.90 V likely corresponds to a further-ring-reduced species. The shoulder observed at approximately −1.80 V, which corresponds to the [**Ni-P**]$^{-/2-}$ couple, increases with benzoic acid concentration, a behavior consistent with the reactivity of the doubly reduced [**Ni-P**]$^{2-}$ dianion.[30] Previous CVs[30,54] of Ni hangman and non-hangman porphyrins in the presence of benzoic acid have also shown an increased current at the monoanion/dianion couple, but with an i/i_p^0 ratio that exceeded the value of 3 observed here in Figure 2b. Additionally, the previously reported Ni porphyrin CVs also featured anodic waves consistent with the −1.47 V feature observed in the Ni phlorin CVs in Figure 2b. This is indicative of Ni isobacteriochlorin generation during CVs of both Ni porphyrins and of Ni phlorins in the presence of benzoic acid. That the Ni porphyrins show HER catalysis from benzoic acid may indicate that [**Ni-Phl**]$^-$ is competent for HER at low concentrations[30] but not here, as the bimolecular disproportionation process that leads to **Ni-iBC** formation will dominate when the Ni phlorin is at high concentrations (as is the case in the CVs shown in Figure 2b).

To drive the reactivity of [**Ni-Phl**]$^-$ with protons, the stronger proton donor tosic acid (pK_a = 8.0 in CH_3CN[55]) was examined. A 17-mL solution of 0.82 mM [**Ni-Phl**]$^-$ in CH_3CN was sealed in a 20-mL vial with a rubber septum stopper and then injected with a molar excess of concentrated tosic acid. The color of the solution rapidly changed from dark brown/yellow to dark purple. The headspace of the vial was analyzed by gas chromatography (GC); no H_2 was detected. In a separate experiment, UV-vis absorption spectra of [**Ni-Phl**]$^-$ were taken before and after excess tosic acid addition (Figure S4). The spectral features corresponding to [**Ni-Phl**]$^-$ rapidly disappear with acid addition, while bands at 399 nm, 520 nm and 555 nm, 598 nm and 621 nm (as a shoulder) appear. An absorption feature at 797 nm appears in several intermediate-time spectra but disappears completely by the final spectrum. The new bands at 399 nm, 520 nm and 555 nm match those of **Ni-P**^{0}, while those at 598 nm and 621 nm belong to Ni(II) isobacteriochlorin (**Ni-iBC**) and Ni (II) chlorin, respectively, based on their similarity to reported spectra.[56]

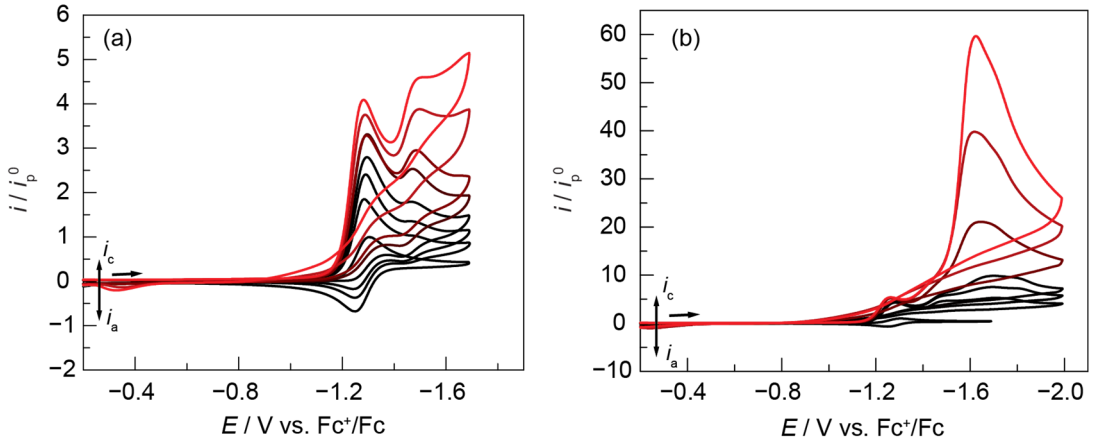

Fig. 3 CVs of **Ni-P** (0.71 mM) in CH_3CN (0.1 M $TBAPF_6$) at a scan rate of 0.1 V s^{-1} (glassy carbon working electrode) in the presence of tosic acid at the following concentrations (from black to red): (a) 0, 0.5, 0.75, 1.0, 1.5, 2.0, 3.5, and 5.0 mM; (b): 0, 5.0, 10.0, 20.0, 35.0 and 50.0 mM.

Electrochemistry of Ni-P in the Presence of Tosic Acid. In view of the lack of H_2 generation and the observed formation of ring-reduced Ni complexes resulting from the reaction of tosic acid with [**Ni-Phl**]$^-$, the electrochemistry of **Ni-P** in the presence of tosic acid was revisited. The cyclic voltammetry of **Ni-P** is presented in Figure 3. Consistent with past reports,[30,54] a reversible one-electron reduction is observed at a standard potential of −1.27 V vs. Fc^+/Fc in the absence of acid. Addition of tosic acid results in a significant increase in the cathodic current at this wave along with a loss of reversibility. At low concentrations of tosic acid (< 5 mM, Figure 3a), this increase in current at the **Ni-P**$^{0/-}$ couple is accompanied by the appearance of a new reversible wave at a potential ~200 mV more negative. This new wave is consistent with the [**Ni-iBC**]$^{0/-}$ couple (*vide infra*) and has a similar current response to that of the one-electron reduction wave of **Ni-P** in the absence of acid. As seen in Figure 3a, this new wave loses reversibility and increases in cathodic current as tosic acid concentrations approach 5 mM. Figure 3b shows CVs of **Ni-P** with increasing concentrations of tosic acid that reach as high as 50.0 mM. At concentrations of tosic acid in excess of 5 mM, the cathodic current at the **Ni-P**$^{0/-}$ couple no longer increases, but the current continues to grow at more negative potentials. The current at the **Ni-P**$^{0/-}$ couple reaches a maximum current ratio (i/i_p^0) of ~4-5 with respect to the one-electron reduction of **Ni-P** in the absence of acid before it ceases to increase in current, as seen in Figure 3b. This suggests that the current at this first wave corresponds to electro-initiated chemical steps rather than catalysis. It should also be noted that CVs at higher concentrations of acid show trace crossing. The crossing suggests that a secondary product (one distinct from **Ni-P** and **Ni-iBC**) is being produced away from the electrode, such as the more reduced Ni hexahydroporphyrins [57] or an electrode-adsorbed material, as discussed in greater detail below.

Controlled-potential bulk electrolysis of **Ni-P** at −1.4 V vs. Fc^+/Fc using a carbon crucible working electrode in the presence of 4.4 equiv of tosic acid was performed to evaluate whether the species produced under reducing and protic conditions was **Ni-iBC**. UV-vis absorption spectra taken during the electrolysis (Figure S5) first showed partial conversion to [**Ni-P**]$^-$ (gray trace), followed by further spectral change, with the Soret band and Q-bands losing intensity along with the concomitant formation of a new band at 598 nm, in agreement with the formation of nickel isobacteriochlorin **Ni-iBC**.

Preparation and Characterization of Ni-iBC. The nickel isobacteriochlorin complex **Ni-iBC** was independently prepared chemically by reducing **Ni-P** to [**Ni-P**]$^-$ via the addition of excess cobaltocene (E^0 = −1.31 vs. Fc^+/Fc)[50] in CH_3CN. Tosic acid was then added to the solution until the UV-vis absorption spectrum no longer changed upon further additions. The initial and final absorption spectra taken during the addition of tosic acid are shown in Figure 4. The final spectrum showed a narrow band at 598 nm along with a broadened Soret band with significantly less intensity than that of the original **Ni-P** species. The product spectrum is consistent with that of **Ni-iBC**.[56] The reaction mixture was brought to dryness under vacuum, re-dissolved in dichloromethane, filtered over a short neutral-alumina column, and brought to dryness again. Proton NMR of the resulting material (Figure S6) was also consistent with an isobacteriochlorin, and high-resolution mass spectrometry (positive ion mode, Figure S7) showed an observed m/z of 1035.01, corresponding to the $M+H^+$ ion of **Ni-iBC** (M = $C_{44}H_{12}F_{20}N_4Ni$, **Ni-iBC**). The UV-vis absorption spectrum of the isolated product showed a small narrow band at 747 nm (Figure S8), which is indicative of a residual amount of the inseparable nickel bacteriochlorin regioisomer. This peak was not observed in the absorption spectra taken during electrochemical (Figure S5) or chemical (Figure 4) preparations of **Ni-iBC**. This observation suggests that a minor amount of isomerization occurs during the purification treatment, likely during the alumina chromatography. The generation of regioisomers has been reported previously during syntheses of tetra-*meso*-aryl isobacteriochlorins.[52,58] The mass spectrometry result cannot distinguish between these two isomers, but the very weak intensity of the 747 nm peak in the UV-vis spectrum (Figure S8) and the presence of only one significant sets of peaks in the NMR spectrum (Figure S6) both indicate that the amount of bacteriochlorin is small.

Cyclic voltammetry of **Ni-iBC** is presented in Figure 5a. A reversible wave is observed centered at −1.46 V vs. Fc^+/Fc. Two other waves are observed, but with very small currents, likely

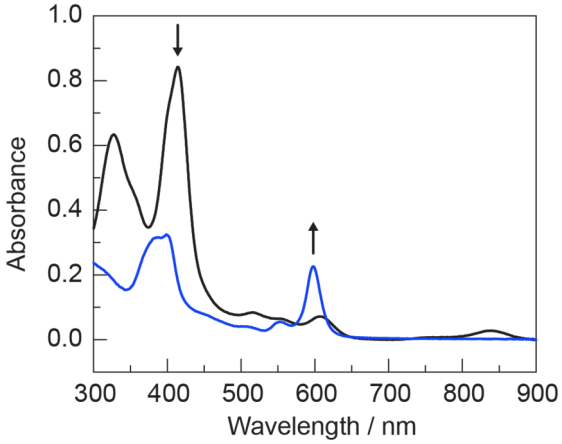

Fig. 4 UV-vis absorption spectra of a solution containing *in situ*-generated [**Ni-P**]$^-$ in the presence of excess cobaltocene before (—) and after (—) the addition of excess tosic acid.

due to the presence of residual impurities such as **Ni-P** or Ni bacteriochlorin. The separation between the cathodic and anodic peak potentials of the observed reversible wave increases at higher scan rates (Figure S9a). This deviation from Nernstian behavior is indicative of a slow electron transfer between the electrode and the complex, and simulation of this scan rate dependence can be used to determine the apparent standard heterogeneous rate constant for electron transfer, k_s^{ap}.[59] The resulting "trumpet" plot for this **Ni-iBC**$^{0/-}$ couple is shown in Figure S9b, and k_s^{ap} is calculated to be 0.014 cm s^{-1}.

As illustrated by the overlaid CVs shown in Figure 5b, the CV wave for the **Ni-iBC**$^{0/-}$ couple at −1.46 V occurs at nearly the exact potential as that observed for the wave that appears in CVs of **Ni-P** upon the addition of small amounts of tosic acid.

The one-electron reduced species [**Ni-iBC**]$^-$ was characterized using thin-layer UV-vis spectroelectrochemistry. Figure 6 shows the spectral evolution for the conversion of **Ni-iBC**^{0} to [**Ni-iBC**]$^-$ with the application of a potential of −1.6 V vs. Fc$^+$/Fc. During this reduction process, the **Ni-iBC**^{0} Soret band (λ_{max} = 383 nm) loses its shoulder at 398 nm and two new shoulders grow in at 336 nm and 360 nm. In the Q-band region, the bands at 503 nm, 553 nm and 598 nm each blue-shift during the reduction, with new bands appearing at 491 nm, 537 nm and 578 nm, respectively. The stability of the reduced [**Ni-iBC**]$^-$ species on the timescale of the spectroelectrochemistry experiment is demonstrated by the reversibility of the electrochemical process. Applying a potential of −0.1 V following generation of [**Ni-iBC**]$^-$ causes the absorption spectra to cleanly convert back to that of **Ni-iBC**^{0} with no loss of intensity (Figure S10).

Electrochemistry of Ni-iBC in the Presence of Tosic Acid. Having established the conversion of **Ni-P** to the ligand-reduced species **Ni-iBC** under hydrogen evolution conditions, attention was turned to the questions of whether the observed **Ni-iBC** was responsible for the catalytic response observed in the CVs of **Ni-P**, and if so, whether **Ni-iBC** is the active catalyst, or alternatively is a precursor to an active catalyst (either molecular or heterogeneous). CVs of **Ni-iBC** in the presence of tosic acid are shown in Figure 7. As shown in Figure S11, the control experiment of tosic acid in the absence of a Ni macrocycle leads to no appreciable current. Upon the addition of acid, the wave for the **Ni-iBC**$^{0/-}$ couple at −1.46 V vs. Fc$^+$/Fc loses reversibility and increases in cathodic current, as shown in Figure 7a. As the concentration of acid is increased, a new, irreversible wave appears at a potential ~150 mV more negative than the **Ni-iBC**$^{0/-}$ couple and grows rapidly, as seen in Figures 7a and 7b. The ratio of observed current to i_p^0 reaches a value over 150 at a tosic acid concentration of 50.0 mM, indicating the presence of efficient catalysis. Bulk electrolysis of **Ni-iBC** in CH_3CN at an applied potential of *ca.* −1.6 V vs. Fc$^+$/Fc in the presence of 30 mM tosic acid demonstrated catalytic production of H_2 with a faradaic efficiency of 86% (see Figure S12). The UV-vis spectrum of the resulting solution still matched that of **Ni-iBC**, with no other new peaks observed except for a broad sloping feature in the far UV, likely due to either the production of a non-macrocyclic species during the bulk electrolysis, or contamination by oxidized species from the counter-electrode compartment during handling of the electrochemical cell following the experiment.

As in the case of the CVs of **Ni-P** in the presence of tosic acid, trace crossing is observed at high concentrations of acid, indicative of a subsequent transformation of **Ni-iBC** upon reduction (forward scan) to a new species that is active for HER at a standard potential positive of [**Ni-iBC**]$^{0/-}$ couple.

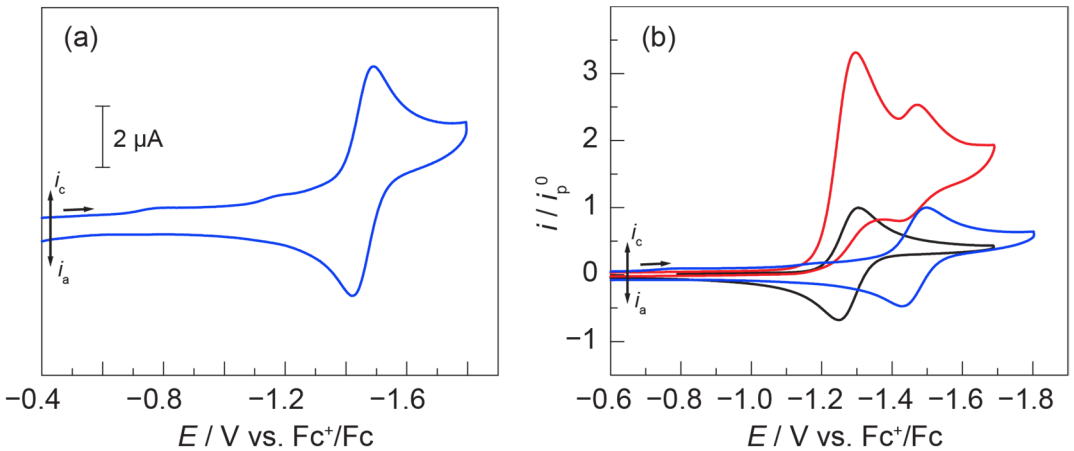

Fig. 5 (a) CV of **Ni-iBC** (0.32 mM) in CH_3CN (0.1 M $TBAPF_6$) at a scan rate of 0.1 V s^{-1} (glassy carbon working electrode). (b) Overlay of normalized CVs of **Ni-P** in the absence of external acid (—), in the presence of 1.5 mM tosic acid (—), and **Ni-iBC** in the absence of external acid (—), all taken in CH_3CN (0.1 M $TBAPF_6$) at a scan rate of 0.1 V s^{-1}.

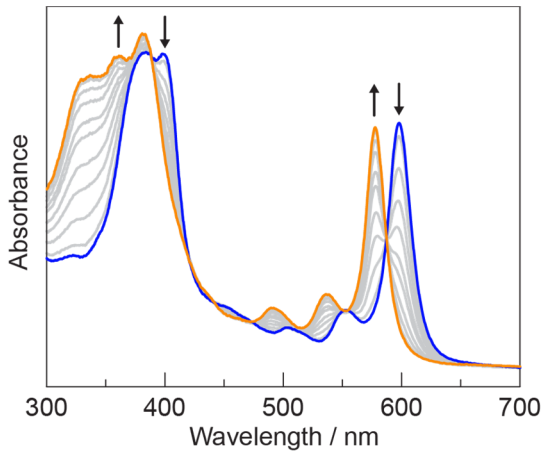

Fig. 6 Thin-layer UV-vis spectroelectrochemistry of **Ni-iBC** in CH_3CN (0.1 M $TBAPF_6$). Potential held at −1.6 V vs. Fc^+/Fc for 200 s. The Ni(II/I) couple is shown with **Ni-iBC** (—) converting to [**Ni-iBC**]$^-$ (—).

Investigation of Heterogeneous Catalytic Behavior. To test for the formation of a catalytically active electrode-adsorbed film upon possible electrochemical degradation of the molecular species, as has been reported for other Ni(II) complexes under reducing and protic conditions,[45–47] rinse tests were performed. After taking CVs in a solution containing 0.71 mM **Ni-P** and 50 mM tosic acid (Figure S14, red trace) and then holding the potential at −1.7 V vs. Fc^+/Fc for 2 min, the glassy carbon working electrode was rinsed with fresh CH_3CN. The electrode was then placed in a new acetonitrile/electrolyte solution containing 50 mM tosic acid but no **Ni-P**. A CV taken in the new solution showed significantly less current (Figure S14, black trace) than the CV taken in the original solution that contained **Ni-P**, though it did show slightly higher current than a CV taken in the fresh solution with a polished glassy carbon working electrode (Figure S14, black trace). However, a rinse test performed with **Ni-iBC** instead of **Ni-P**, shown in Figure S15, demonstrates a catalytic response of the rinsed electrode in fresh solution (black trace) that is comparable to that of the original solution that contained the **Ni-iBC** (red trace). This response indicates the presence of a surface-adsorbed, catalytically active species. Similar experiments with the weaker acid, trifluoroacetic acid, show similar phenomena with regard to trace crossing and deposition of heterogeneous material as in the case of tosic acid, but to a lesser extent, as shown in Figures S16-S17. A rinse test was then performed with $Ni(ClO_4)_2•6H_2O$ in CH_3CN. CVs of $Ni(ClO_4)_2$ in the presence of tosic acid are shown in Figure S18, and demonstrate a catalytic response at approximately −1.9 V, along with trace crossing similar to that observed in CVs of **Ni-P** and **Ni-iBC** (see Figures 3 and 7, respectively). A CV of the rinsed electrode in fresh solution containing tosic acid but no $Ni(ClO_4)_2•6H_2O$ following electrolysis in $Ni(ClO_4)_2•6H_2O$ showed a catalytic response (Figure S19), and a comparison of the CVs from rinse tests of the **Ni-iBC** and $Ni(ClO_4)_2•6H_2O$ show similar responses, as shown in Figure S20. This suggests that the reduction of Ni^{2+} in CH_3CN produces the same species that is responsible for at least a significant portion of the catalytic response observed during electrolysis of **Ni-iBC**. The common observations of catalytic activity during the rinse tests and trace crossing in the CVs of **Ni-iBC** and $Ni(ClO_4)_2•6H_2O$ are consistent with the production of an at least partially-insoluble Ni-containing species upon the forward CV scans during reduction of **Ni-iBC** that is catalytically active with a standard potential more positive than the **Ni-iBC**$^{0/-}$ couple.

To better characterize the active material deposited on the electrode, glassy carbon plates were electrolyzed in solutions containing either $Ni(ClO_4)_2•6H_2O$ or **Ni-iBC** in the presence of 20 mM tosic acid for 10 min at a potential of −1.7 V vs. $Fc^{+/0}$. XPS spectra of the glassy carbon plates were then acquired, as shown in Figure 8. The XPS spectra acquired from the glassy carbon plates electrolyzed in $Ni(ClO_4)_2•6H_2O$ (Figure 9a) and **Ni-iBC** (Figure 9b) showed almost the identical peaks in terms of pattern and positions in the Ni 2P region, confirming the presence of a common electrode absorbed species produced in each case. Notably, the predominant peak observed is at around 856 eV, which corresponds to a $Ni(OH)_2$ species, rather than a Ni^0 species.

Discussion

Scheme 1 summarizes the reactivity of **Ni-P** under hydrogen evolving conditions based on the electrochemical and spectroscopic data presented in this study. The scheme comprises a ligand-based $L_n(H^+)M(e^-)$ PCET process

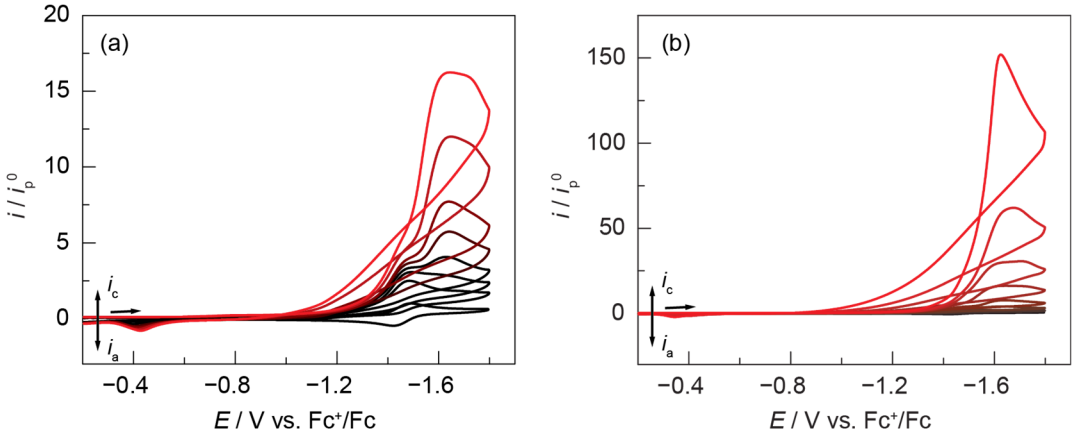

Fig. 7 CVs of **Ni-iBC** (0.32 mM) in CH_3CN (0.1 M $TBAPF_6$) at a scan rate of 0.1 V s^{-1} (glassy carbon working electrode) in the presence of tosic acid at the following concentrations (from black to red): (a) 0, 0.5, 0.75, 1.0, 2.0, 3.5, and 5.0 mM; (b) 0, 0.5, 1.0, 2.0, 5.0, 10.0, 20.0, and 50.0 mM.

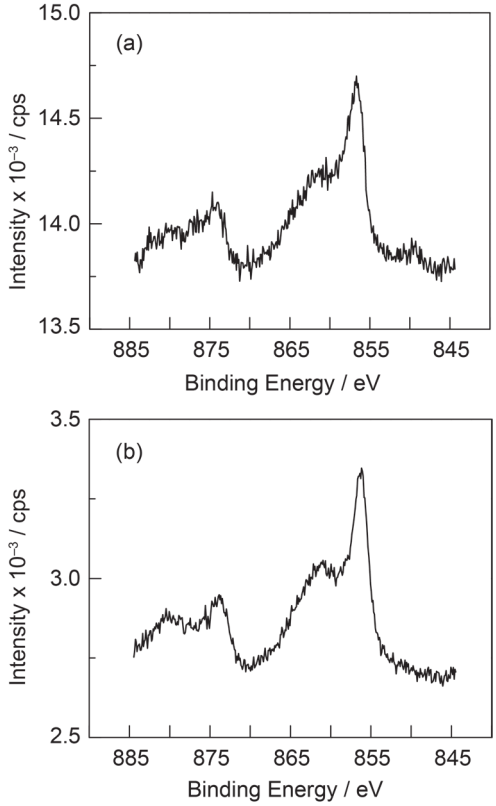

Fig. 8 XPS spectra of glassy carbon plate electrode taken following bulk electrolysis at a potential of −1.7 V for 10 min in the presence of (a) $Ni(ClO_4)_2 \cdot 6H_2O$ (0.5 mM) and tosic acid (20 mM) in CH_3CN (0.1 M $TBAPF_6$), and (b)) **Ni-iBC** (0.5 mM) and tosic acid (20 mM) in CH_3CN (0.1 M $TBAPF_6$)

beginning with **Ni-P** and leading to the formation of the Ni isobacteriochlorin **Ni-iBC.**

The **Ni-P** exhibits a proclivity for ligand-based PCET to produce the phlorin anion [**Ni-Phl**]⁻. The redox-induced protonation of the ring is clearly demonstrated by the observation of the distinctive near-IR spectroscopic signature of phlorin anion [**Ni-Phl**]⁻ upon stoichiometric addition of a proton donor to doubly-reduced [**Ni-P**]²⁻ (Figure 1b). This result is in accordance with the mechanism proposed by Hammes-Schiffer based on the results of DFT calculations.[30] We see no evidence that the reduced phlorin [**Ni-Phl**]⁻ is capable of supporting HER under the conditions reported herein, where we are at the near mM concentration of macrocycle where disproportionation is preferred; at low macrocycle concentrations the Ni phlorin may well support HER as has been previously discussed. The normalized cathodic current response of [**Ni-Phl**]⁻ in the presence of acid gives a ratio of ~3 (Figure 2b), indicative of a chemical process involving further reduction of [**Ni-Phl**]⁻ by three electrons as opposed to a chemical process encompassing HER catalysis. Rather, the role of phlorin anion is to provide a facile pathway to β-hydrogenation of the macrocyclic ring to produce **Ni-iBC**. Figure S4 supports a mechanism in which **Ni-iBC** is produced from [**Ni-Phl**]⁻ by an acid-induced disproportionation reaction, as essentially equimolar amounts of **Ni-P** and **Ni-iBC** are produced upon the addition of acid. The overall reaction sequence to produce **Ni-iBC** from **Ni-P** is thus,

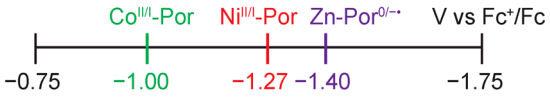

Fig. 9 Standard reduction potentials of **Co-P** (green, from Ref 29, **Ni-P** (red), and **Zn-P** (purple).

$$\textbf{Ni-P} + 2e^- + H^+ \rightarrow [\textbf{Ni-Phl}]^- \quad (1)$$

$$2[\textbf{Ni-Phl}]^- + 2H^+ \rightarrow \textbf{Ni-iBC} + \textbf{Ni-P} \quad (2)$$

Under the reducing conditions of HER, the **Ni-P** produced from eq (2) will be driven through continually to **Ni-iBC**, thus completing the four electron, four proton process. Eq 2 describes a net addition of two electrons and three protons to a [**Ni-Phl**]⁻ anion to form **Ni-iBC** (the second equivalent of [**Ni-Phl**]⁻ provides two electrons and one proton, while the other two protons are provided by the external acid). In an electrochemical experiment, the electrons may be provided heterogeneously from the electrode as well. Scheme 1 shows the $2e^-$, $3H^+$ stoichiometry without specifying mechanism. Prototropic rearrangement of phlorins to chlorins (and chlorin-phlorins to isobacteriochlorins) is a known phenomenon, and an example of a possible intermolecular tautomerization mechanism is shown in Lindsey's review of chlorin synthesis.[37]

The ligand-based PCET reactivity of **Ni-P** is a consequence of the formal reduction potential of the porphyrin ring (Figure 9), which is provided by a **Zn-P** reference. In the absence of a redox-active metal, the reversible one-electron redox couple for **Zn-P** at −1.40 V (Figure S21) is reliably assigned to porphyrin macrocycle reduction. In the case of **Ni-P**, the one-electron reduction of the metal is E(**Ni$^{II/I}$-P**) = −1.27 V, providing a separation of only 130 mV from porphyrin ligand reduction. Simple energetic considerations indicate that with this difference in potential, ~1% of the reduced π-radical anions are thermally-accessible by intramolecular electron transfer from the metal(I) center to the macrocycle π orbitals, offering a pathway for the ligand protonation at the *meso* carbon. Conversely, the standard potential for the reduction of **Co-P** is 400 mV more positive (E(**Co$^{II/I}$-P**) = −1.00 V vs. Fc^+/Fc,[29]) than that of the porphyrin π-system. At this large potential difference, population of the π-radical anion state via intramolecular ET to the porphyrin ligand is negligible, leaving metal-hydride formation as the only thermally-accessible protonation pathway. Indeed, phlorin is not observed or predicted as a reaction intermediate in **Co-P** HER chemistry (with strong acids) and the mechanism of HER is entirely consistent with an $L_nM(e^-,H^+)$ process to yield a Co(III)-hydride.[29]

The [**Ni-Phl**]⁻ provides entry to **Ni-iBC**, which itself could serve as either the active catalytic species or as a precatalyst that ultimately generates an active heterogeneous material on the electrode. The formation of **Ni-iBC** (and subsequent conversion) was outside the scope of previous DFT analysis of the **Ni-P** system. The origins of HER electroactivity derived from **Ni-iBC** is clarified with independently-synthesized **Ni-**

Scheme 1. Hydroporphyin formation from **Ni-P** under hydrogen evolving conditions.

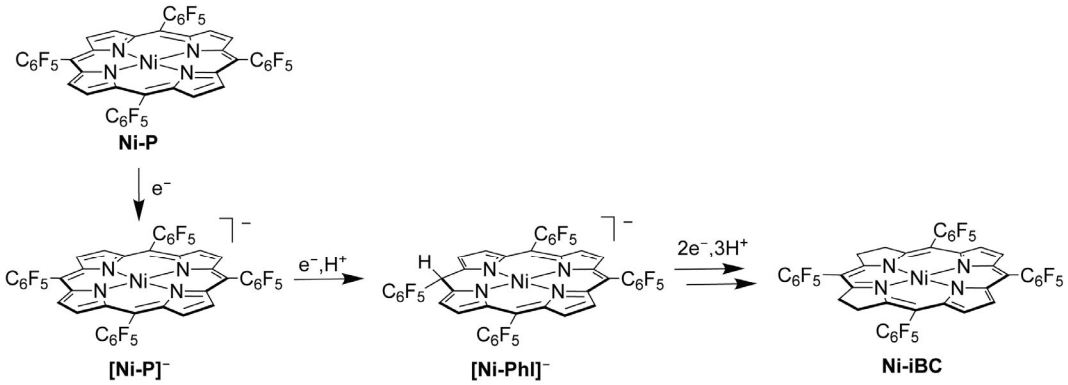

iBC, which forms readily via the addition of excess reducing equivalents and tosic acid to **Ni-P** (Figures 4 and S5). CVs of the titration of tosic acid to **Ni-iBC** show the appearance of significant catalysis (Figure 7), which is confirmed to be HER based on the detection of H_2 by GC (Figure S12). In light of these results, the CV response of **Ni-P** in the presence of tosic acid, shown in Figure 3, is elucidated. The initial rise in current at the **Ni-P**$^{0/-}$ couple at –1.27 V is not catalytic but instead corresponds to the four-electron, four-proton reduction of the porphyrin to the isobacteriochlorin. The near-quantitative formation of **Ni-iBC** can be inferred from the appearance of the reversible wave centred at –1.46 V that corresponds to the **Ni-iBC**$^{0/-}$ couple as verified by the comparison to the CV of independently prepared **Ni-iBC** (Figure 5b). With the exception of the extent to which trace crossing is observed, the HER catalytic response shown in the CV of **Ni-P** in Figure 3 matches the catalytic HER response from the **Ni-iBC**$^{0/-}$ of independently-prepared **Ni-iBC** (Figure 7), confirming **Ni-iBC** as a key species in the HER mechanism, regardless of whether the initial complex is the porphyrin or the isobacteriochlorin.

Even considering only homogeneous reactivity, the precise sequence of electron transfers and proton transfers in Scheme 1 should be dependent on the strength of the acid. This can be seen in the cyclic voltammetry results (here and in ref 30), where tosic acid (pK_a 8.0) and trifluoroacetic acid (pK_a 12.7) initiate chemistry at the [**Ni-P**]$^{0/-}$ couple, while acids like benzoic acid (pK_a 20.7) and phenol (pK_a 29.1) require a second reduction to [**Ni-P**]$^{2-}$ in order to protonate the complex. This implies that the pK_a of the protonated **Ni-P** monoanion lies between 12.7 and 20.7. The CVs in Figure 2b indicate that acids as weak as benzoic acid are capable of driving **Ni-iBC** formation from [**Ni-Phl**]$^-$, but hydrogen generation (either via **Ni-iBC** or a resulting Ni-based heterogeneous species) requires a stronger acid. This suggests that the step that requires the greatest acidity is metal-hydride formation (either in a homogeneous complex or an electrode-adsorbed species) rather than a ligand protonation.

The rinse tests shown in Figures S15 and S17 show the formation of a significant amount of electrode-adsorbed material capable of HER catalysis during the electrochemical reduction of **Ni-iBC** in the presence of acid, which greatly complicates evaluation of **Ni-iBC** as an active HER catalyst. Rinses tests under similar conditions with the Ni^{2+} salt $Ni(ClO_4)_2{\bullet}6H_2O$ show a similar electrocatalytic response, and XPS confirms production of a catalytically-active Ni-based heterogeneous species in both cases. The degree to which the catalysis under strong acidic conditions can be attributed to homogeneous vs. heterogeneous phenomena is difficult to determine. On the one hand, the rinse tests shown in Figures S15 and S17 clearly show that the nickel-containing electrode-adsorbed material is catalytically competent for HER. However, previous reports have demonstrated clean thermal hydrogen generation from homogeneous solutions of reduced Ni isobacteriochlorin upon the addition of acid (with concomitant regeneration of Ni(II) isobacteriochlorin).[60]

The observed trace-crossing in the CVs and the appearance of electrode-adsorbed species are likely related, and the extent to which each are observed is dependent on the proton activity of the solution, as is seen by their dependence on the acid strength in Figures 7 and S15-S17. We note that it is not interconversion between **Ni-P** and **Ni-iBC** that is responsible for the observed trace crossing. As mentioned above, the initial product of this side-reactivity is likely a further ring-reduced complex such as a hexahydroporphyrin, though this species likely rapidly leads to the release of Ni^{2+} ions that contribute to the formation of an electrode-adsorbed species, as similar trace crossing is observed during reduction of $Ni(ClO_4)_2{\bullet}6H_2O$. Hexahydroporphyrins such as the isobacteriochlorin-phlorin-like nickel 1,2,3,7,8,20-hexahydroporphyrins are prone to demetalation under harshly acidic conditions.[57] Alternatively, Dempsey has proposed insertion into ligand-ligand bonds by Ni-hydrides as a means for decomposition of Ni complexes into surface-adsorbed species under HER conditions.[46] More generally, Dempsey has also shown precedence for ligand hydrogenation as being a key initial step during the degradation of molecular Ni complexes into nickel-containing heterogeneous material,[47] a conclusion that is wholly consistent with the behaviour of **Ni-P** and **Ni-iBC** studied in this work.

Conclusions

Reduction of the nickel porphyrin complex **Ni-P** in the presence of strong proton donors leads to the formation of ring-reduced Ni hydroporphyrins rather than Ni-hydrides, underscoring the importance of ligand-based PCET processes during HER catalysis. The first protonation of reduced **Ni-P** occurs at the *meso* carbon, ultimately forming a Ni phlorin anion [**Ni-Phl**]$^-$, which has been synthesized, isolated, and

characterized. Reaction of the phlorin anion with strong acid leads to further saturation of the ring, rapidly forming the Ni isobacteriochlorin **Ni-iBC**. Upon reduction at high concentrations of strong acid, **Ni-iBC** decomposes to form a catalytically active, nickel-containing material that adsorbs to the surface of the electrode, underscoring the role that ligand hydrogenation can play in forming heterogeneous catalysts during harsh HER conditions.

The HER chemistry of a complex Ni porphyrin/hydroporphyrin system is underpinned by a non-innocent ligand framework. The degree to which the macrocycle ligand participates directly in PCET reactions depends on an interplay between the reduction potentials of the metal and the macrocycle ligand (which in turn depend on the substituents on the macrocycle), as well as the acid strength. This complexity is particularly striking with Ni. In weaker acids, Ni porphyrins supports HER[54] whereas the stronger acids drive effectively hydrogenation of the macrocycle by PCET, as we show here. The participation of the macrocyclic ring in PCET chemistry is largely a consequence of the electronic structure of metal. Porphyrin complexes comprising earlier first row transition metals (Co(II) and earlier) have empty or partially-filled $3d_{z^2}$ orbitals and can therefore undergo metal-centered reduction and consequently metal-hydride formation. Conversely, the $3d_{z^2}$ orbital of d^8 Ni(II) centers is filled and any additional electrons are relegated to populating the higher-energy $3d_{x^2-y^2}$ orbital. Any low-lying ligand orbitals will therefore make ligand non-innocent reactivity a possibility, especially for Ni macrocyclic complexes under reducing conditions.

ASSOCIATED CONTENT

Supporting Information

Summaries of ^{1}H NMR spectra, high-resolution MS spectra, cyclic voltammograms, results of rinse test and Faradaic yield measurements are presented in the Supporting Information. This material is available free of charge via the Internet at http://pubs.acs.org.

AUTHOR INFORMATION

Corresponding Author

E-mail: dnocera@fas.harvard.edu

ACKNOWLEDGMENT

We thank Dr. Dilek K. Dogutan and Dr. Cyrille Costentin for helpful discussions, Dr. Joseph S. Elias for performing the XPS experiments, and Christopher M. Lemon for providing **Zn-P**. This material is based upon work supported under the Solar Photochemistry Program of the Chemical Sciences, Geosciences and Biosciences Division, Office of Basic Energy Sciences of the U. S. Department of Energy DE-SC0017619.

References

1 N. S. Lewis, D. G. Nocera, *Proc. Natl. Acad. Sci. U. S. A.*, 2006, **103**, 15729–15735. Powering the Planet: Chemical Challenges in Solar Energy Utilization.

2 D. G. Nocera, *Inorg. Chem.*, 2009, **48**, 10001–10017. Chemistry of Personalized Solar Energy.

3 T. R. Cook, D. K. Dogutan, S. Y. Reece, Y. Surendranath, T. S. Teets, D. G. Nocera, *Chem. Rev.* 2010, **110**, 6474–6502. Solar Energy Supply and Storage for the Legacy and Nonlegacy Worlds.

4 R. I. Cukier, D. G. Nocera, *Annu. Rev. Phys. Chem.*, 1998, **49**, 337–369. Proton-Coupled Electron Transfer.

5 J. M. Mayer, *Annu. Rev. Phys. Chem.*, 2004, **55**, 363–390. Proton-Coupled Electron Transfer: A Reaction Chemist's View.

6 M. H. V. Huynh, T. J. Meyer, *Chem. Rev.*, 2007, **107**, 5004–5064. Proton-Coupled Electron Transfer.

7 C. Costentin, *Chem. Rev.*, 2008, **108**, 2145–2179. Electrochemical Approach to the Mechanistic Study of Proton-Coupled Electron Transfer.

8 S. Hammes-Schiffer, *Acc. Chem. Res.*, 2009, **42**, 1881–1889. Theory of Proton-Coupled Electron Transfer in Energy Conversion Processes.

9 X. Hu, B. S. Brunschwig, J. C. Peters, *J. Am. Chem. Soc.*, 2007, **129**, 8988–8998. Electrocatalytic Hydrogen Evolution at Low Overpotentials by Cobalt Macrocyclic Glyoxime and Tetraimine Complexes.

10 J. L. Dempsey, B. S. Brunschwig, J. R. Winkler, H. B. Gray, *Acc. Chem. Res.* 2009, **42**, 1995–2004. Hydrogen Evolution Catalyzed by Cobaloximes.

11 N. Kaeffer, M. Chavarot-Kerlidou, V. Artero, *Acc. Chem. Res.*, 2015, **48**, 1286–1295. Hydrogen Evolution Catalyzed by Cobalt Diimine-dioxime Complexes.

12 M. R. DuBois, D. L. DuBois, *Chem. Soc. Rev.*, 2008, **38**, 62–72. The Roles of the First and Second Coordination Spheres in the Design of Molecular Catalysts for H_2 Production and Oxidation.

13 M. L. Helm, M. P. Stewart, R. M. Bullock, M. R. DuBois, D. L. DuBois, *Science*, 2011, **333**, 863–866. A Synthetic Nickel Electrocatalyst with a Turnover Frequency above 100,000 s^{-1} for H_2 Production.

14 W. R. McNamara, Z. Han, P. J. Alperin, W. W. Brennessel, P. L. Holland, R. Eisenberg, *J. Am. Chem. Soc.*, 2011, **133**, 15368–15371. A Cobalt-Dithiolene Complex for the Photocatalytic and Electrocatalytic Reduction of Protons.

15 F. Gloaguen, T. B. Rauchfuss, *Chem. Soc. Rev.*, 2009, **38**, 100–108. Small Molecule Mimics of Hydrogenases: Hydrides and Redox.

16 P. Du, R. Eisenberg, *Energy Environ. Sci.*, 2012, **5**, 6012–6021. Catalysts Made of Earth-Abundant Elements (Co, Ni, Fe) for Water Splitting: Recent Progress and Future Challenges.

17 C. Y. Yeh, C. J. Chang and D. G. Nocera, *J. Am. Chem. Soc.*, 2001, **123**, 1513–1514. "Hangman" Porphyrins for the Assembly of a Model Heme Water Channel.

18 D. K. Dogutan, D. K. Bediako, T. S. Teets, M. Schwalbe, D. G. Nocera, D., *Org. Lett.*, 2010, **12**, 1036–1039. Efficient Synthesis of Hangman Porphyrins.

19 D. K. Dogutan, D. K. Bediako, D. J. Graham, C. M. Lemon, D. G. Nocera, *J. Porphyrins Phthalocyanines*, 2015, **19**, 1–8. Proton-Coupled Electron Transfer Chemistry of Hangman Macrocycles: Hydrogen and Oxygen Evolution Reactions.

20 A. D. Wilson, R. K. Shoemaker, A. Miedaner, J. T. Muckerman, D. L. DuBois, M. R. DuBois, *Proc. Natl. Acad. Sci. U. S. A.*, 2007, **104**, 6951–6956. Nature of Hydrogen Interactions with Ni(II) Complexes Containing Cyclic Phosphine Ligands with Pendant Nitrogen Bases.

21 S. Ezzaher, J.-F. Capon, F. Gloaguen, F. Y. Pétillon, P. Schollhammer, J. Talarmin, N. Kervarec, *Inorg. Chem.*, 2009, **48**, 2–4. Influence of a Pendant Amine in the Second Coordination Sphere on Proton Transfer at a Dissymmetrically Disubstituted Diiron System Related to the $[2Fe]_H$ Subsite of $[FeFe]H_2$ase.

22 S. Chatterjee, K. Sengupta, B. Mondal, S. Dey, A Dey, *Acc. Chem. Res.*, 2017, **50**, 1744–1753. Factors Determining the Rate and Selectivity of $4e^-/4H^+$ Electrocatalytic Reduction of Dioxygen by Iron Porphyrin Complexes.

23 A. Rana, B. Mondal, P. Sen, S. Dey, A. Dey, *Inorg. Chem.*, 2017, **56**, 1783–1793. Activating Fe(I) Porphyrins for the Hydrogen Evolution Reaction Using Second-Sphere Proton Transfer Residues.

24 B. H. Solis, S. Hammes-Schiffer, *J. Am. Chem. Soc.*, 2012, **134**, 15253–15256. Computational Study of Anomalous Reduction Potentials for Hydrogen Evolution Catalyzed by Cobalt Dithiolene Complexes.

25 L. M. A. Quintana, S. I. Johnson, S. L. Corona, W. Villatoro, W. A. Goddard, M. K. Takase, D. G. VanderVelde, J. R. Winkler, H. B. Gray, J. D. Blakemore, *Proc. Natl. Acad. Sci. U. S. A.*, 2016, **113**, 6409–6414. Proton–Hydride Tautomerism in Hydrogen Evolution Catalysis.

26 S. I. Johnson, H. B. Gray, J. D. Blakemore, W. A. Goddard, *Inorg. Chem.*, 2017, **56**, 11375–11386. Role of Ligand Protonation in Dihydrogen Evolution from a Pentamethylcyclopentadienyl Rhodium Catalyst.

27 A. Z. Haddad, S. P. Cronin, M. S. Mashuta, R. M. Buchanan, C. A. Grapperhaus, *Inorg. Chem.*, 2017, **56**, 11254–11265. Metal-Assisted Ligand-Centered Electrocatalytic Hydrogen Evolution upon Reduction of a Bis(thiosemicarbazonato)Cu(II) Complex.

28 T. J. Sherbow, J. C. Fettinger, L. A. Berben, *Inorg. Chem.*, 2017, **56**, 8651–8660. Control of Ligand pK_a Values Tunes the Electrocatalytic Dihydrogen Evolution Mechanism in a Redox-Active Aluminum(III) Complex.

29 B. H. Solis, A. G. Maher, T. Honda, D. C. Powers, D. G. Nocera, S. Hammes-Schiffer, *ACS Catal.*, 2014, **4**, 4516–4526. Theoretical Analysis of Cobalt Hangman Porphyrins: Ligand Dearomatization and Mechanistic Implications for Hydrogen Evolution.

30 Solis, A. G. Maher, D. K. Dogutan, D. G. Nocera, S. Hammes-Schiffer, *Proc. Natl. Acad. Sci. U. S. A.*, 2016, **113**, 485–492. Nickel Phlorin Intermediate Formed by Proton-Coupled Electron Transfer in Hydrogen Evolution Mechanism.

31 Y. Han, H. Fang, H. Jing, H. Sun, H. Lei, W. Lai, R. Cao, *Angew. Chem.*, 2016, **128**, 5547–5462. Singly versus Doubly Reduced Nickel Porphyrins for Proton Reduction: Experimental and Theoretical Evidence for a Homolytic Hydrogen-Evolution Reaction.

32 D. Mauzerall, *J. Am. Chem. Soc.*, 1962, **84**, 2437–2445. The Photoreduction of Porphyrins: Structure of the Products.

33 G. L. Closs, L. E. Closs, *J. Am. Chem. Soc.*, 1963, **85**, 818–819. Negative Ions of Porphin Metal Complexes.

34 G. S. Wilson, G. Peychal-Heiling, *Anal. Chem.*, 1971, **43**, 545–550. Electrochemical Studies of Some Porphyrin IX Derivatives in Aprotic Media.

35 H. W. Whitlock, M. Y. Oester, *J. Am. Chem. Soc.*, 1973, **95**, 5738–5741. Chemistry of Porphyrins. IV. Behavior of Di- and Tetrahydroporphyrins under Alkaline Donditions. Direct Observation of the Chlorin-Phlorin Equilibrium.

36 H. Scheer, in *The Porphyrins;* ed. D. Dolphin, Academic Press, New York, 1978; vol. II, ch. 1, pp 18–22.

37 M. Taniguchi, J. S. Lindsey, *Chem. Rev.*, 2017, **117**, 344–535. Synthetic Chlorins, Possible Surrogates for Chlorophylls, Prepared by Derivatization of Porphyrins.

38 S. Salzl, M. Ertl, G. Knor, *Phys. Chem. Chem. Phys.*, 2017, **19**, 8141–8147. Evidence for Photosensitised Hydrogen Production from Water in the Absence of Precious Metals, Redox-Mediators and Co-Catalysts.

39 Z.-Y. Wu, T. Wang, Y.-S. Meng, Y. Rao, B.-W. Wang, J. Zheng, S. Gao and J.-L. Zhang, *Chem. Sci.*, 2017, **8**, 5953–5961. Enhancing the Reactivity of Nickel(II) in Hydrogen Evolution Reactions (HERs) by β-Hydrogenation of Porphyrinoid Ligands.

40 J. Jiang, A. J. Matula, J. R. Swierk, N. Romano, Y. Wu, V. S. Batista, R. H. Crabtree, J. S. Lindsey, H. Wang, and G. W. Brudvig, *ACS Catal.*, 2018, **8**, 10131–10136. Unusual Stability of a Bacteriochlorin Electrocatalyst under Reductive Conditions. A Case Study on CO_2 Conversion to CO.

41 A. Ogawa, K. Oohara, and T. Hayashi, Inorg. Chem, 2018, **57**, 14644–11652. Synthesis and Characterization of meso-Substituted Cobalt Tetradehydrocorrin and Evaluation of Its Electrocatalytic Behavior Toward CO_2 Reduction and H_2 Evolution.

42 E. Anxolabéhère-Mallart, C. Costentin, M. Fournier, S. Nowak, M. Robert and J.-M. Savéant, *J. Am. Chem. Soc.*, 2012, **134**, 6104–6107. Boron-Capped Tris(glyoximato) Cobalt Clathrochelate as a Precursor for the Electrodeposition of Nanoparticles Catalyzing H_2 Evolution in Water.

43 S. El Ghachtouli, R. Guillot, F. Brisset, A. Aukauloo, *ChemSusChem*, 2013, **6**, 2226–2230. Cobalt-Based Particles Formed upon Electrocatalytic Hydrogen Production by a Cobalt Pyridine Oxime Complex.

44 E. Anxolabéhère-Mallart, C. Costentin, M. Fournier and M. Robert, *J. Phys. Chem. C*, 2014, **118**, 13377–13381. Cobalt-Bisglyoximato Diphenyl Complex as a Precatalyst for Electrocatalytic H_2 Evolution.

45 S. Cherdo, S. E. Ghachtouli, M. Sircoglou, F. Brisset, M. Orio and A. Aukauloo, *Chem. Commun.*, 2014, **50**, 13514–13516. A Nickel Dimethyl Glyoximato Complex to Form Nickel Based Nanoparticles for Electrocatalytic H_2 Production.

46 D. J. Martin, B. D. McCarthy, C. L. Donley and J. L. Dempsey, *Chem. Commun.*, 2015, **51**, 5290–5293. Electrochemical Hydrogenation of a Homogeneous Nickel Complex to Form a Surface Adsorbed Hydrogen-Evolving Species.

47 B. D. McCarthy, C. L. Donley, J. L. Dempsey, *Chem. Sci.*, 2015, **6**, 2827–2834. Electrode Initiated Proton-Coupled Electron Transfer to Promote Degradation of a Nickel(II) Coordination Complex.

48 M. J. Rudolf, *J. Electroanal. Chem.*, 2003, **543**, 23–39. DigiElch from Elchsoft under http://www.elchsoft.com.

49 D. C. Powers, M. B. Chambers, T. S. Teets, N. Elgrishi, B. L. Anderson, D. G. Nocera, *Chem. Sci.*, 2013, **4**, 2880–2885. Halogen Photoelimination from Dirhodium Phosphazane Complexes via Chloride-Bridged Intermediates.

50 N. G. Connelly, W. E. Geiger, *Chem. Rev.*, 1996, **96**, 877–910. Chemical Redox Agents for Organometallic Chemistry.

51 A. Kütt, V. Movchun, T. Rodima, T. Dansauer, E. B. Rusanov, I. Leito, I. Kaljurand, J. Koppel, V. Pihl, I. Koppel, G. Ovsjannikov, L. Toom, M. Mishima, M. Medebielle, E. Lork, G.-V. Röschenthaler, I. A. Koppel, A. A. Kolomeitsev, *J. Org. Chem.*, 2008, **73**, 2607–2620. Pentakis(trifluoromethyl)phenyl, a Sterically Crowded and Electron-withdrawing Group: Synthesis and Acidity of Pentakis(trifluoromethyl)benzene, -toluene, -phenol, and -aniline.

52 A. M. Stolzenberg, M. T. Stershic, *J. Am. Chem. Soc.*, 1988, **110**, 6391–6402. Reductive Chemistry of Nickel Hydroporphyrins. Evidence for a Biologically Significant Difference between Porphyrins, Hydroporphyrins, and Other Tetrapyrroles.

53 Y. Fang, Y. G. Gorbunova, P. Chen, X. Jiang, M. Manowong, A. A. Sinelshchikova, Y. Y. Enakieva, A. G. M.artynov, A. Y. Tsivadze, A. Bessmertnykh-Lemeune, C. Stern, R. Guilard, K. M. Kadish, *Inorg. Chem.*, 2015, **54**, 3501–3512. Electrochemical and Spectroelectrochemical Studies of Diphosphorylated Metalloporphyrins. Generation of a Phlorin Anion Product.

54 D. K. Bediako, B. H. Solis, D. K. Dogutan, M. M. Roubelakis, A. G. Maher, C. H. Lee, M. B. Chambers, S. Hammes-Schiffer, D. G. Nocera, *Proc. Natl. Acad. Sci. U. S. A.*, 2014, **111**, 15001–15006. Role of Pendant Proton Relays and Proton-Coupled Electron Transfer on the Hydrogen Evolution Reaction by Nickel Hangman Porphyrins.

55 K. Izutsu, *Acid-Base Dissociation Constants in Dipolar Aprotic Solvents*, Blackwell, Boston, 1990.

56 M. Dommaschk, V. Thoms, C. Schütt, C. Näther, R. Puttreddy, K. Rissanen, R. Herges, *Inorg. Chem.*, 2015, **54**, 9390–9392. Coordination-Induced Spin-State Switching with Nickel Chlorin and Nickel Isobacteriochlorin.

57 G. K. Lahiri, A. M. Stolzenberg, *Angew. Chem. Int. Ed.*, 1993, **32**, 429–432. Facile Formation of Hexahydroporphyrin Complexes by Reduction of Octaethylisobacteriochlorinnickel(II).

58 Y. Yu, T. Furuyama, J. Tang, Z.-Y. Wu, J.-Z. Chen, N. Kobayashi, J.-L. Zhang, *Inorg. Chem. Front.*, 2015, **2**, 671–677. Stable Iso-

bacteriochlorin Mimics from Porpholactone: Effect of a β-Oxazolone Moiety on the Frontier π-Molecular Orbitals.

59 J.-M. Savéant, *Elements of Molecular and Biomolecular Electrochemistry: an Electrochemical Approach to Electron Transfer Chemistry*, John Wiley, Hoboken, NJ, 2006.

60 G. K. Lahiri, L. J. Schussel and A. M. Stolzenberg, *Inorg. Chem.*, 1992, **31**, 4991–5000. F430 Model chemistry. Mechanistic Investigation of the Reduction, Coupling, and Dehydrohalogenation of Alkyl Halides by the Nickel(I) Octaethylisobacteriochlorin Anion.

Synopsis: Proton-coupled electron transfer reaction of an electron-deficient Ni porphyrin in acid undergoes a ligand non-innocence chemistry. Initial electron transfer is accompanied by protonation of the ring to produce a phlorin, which then undergoes further reduction and protonation steps to produce a Ni isobacteriochlorin. The Ni isobacteriochlorin is the species responsible for hydrogen evolution, but under strongly acidic conditions, the HER catalysis arises from conversion of the Ni isobacteriochlorin into a nickel-containing, catalytically active electrode-adsorbed species.

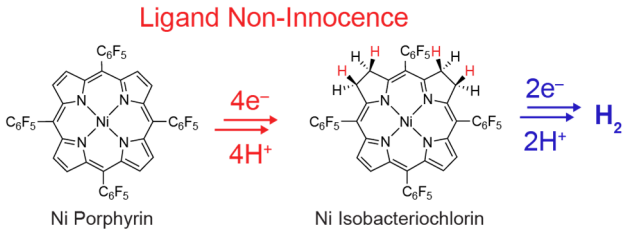

Supplementary Information

Ligand Non-innocence in Nickel Porphyrins: Nickel Isobacteriochlorin Formation Under Hydrogen Evolution Conditions

Andrew G. Maher, Mengran Liu, and Daniel G. Nocera*

Department of Chemistry and Chemical Biology, 12 Oxford Street, Harvard University, Cambridge, MA 02138-2902 U.S.A.

* dnocera@fas.harvard.edu

Index *Page*

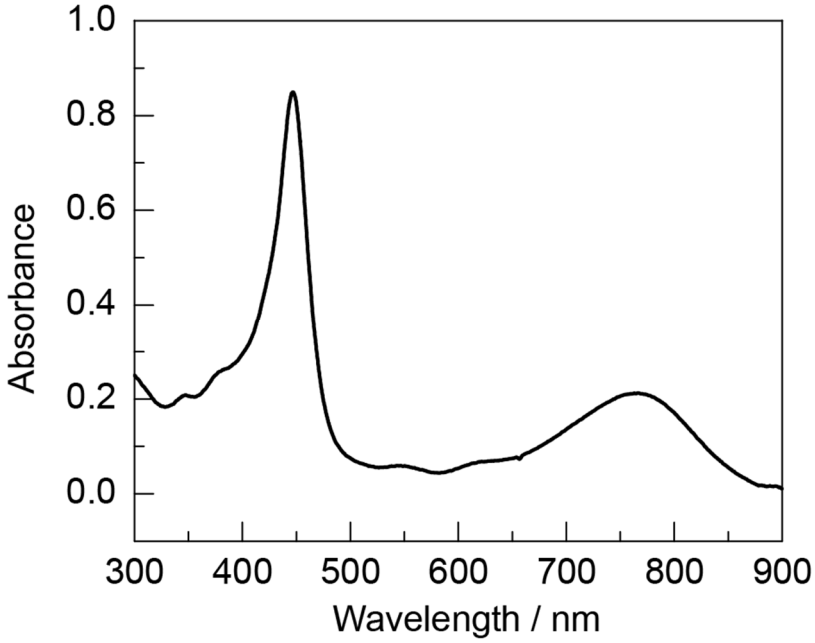

Figure S1. UV-vis absorption spectrum of **[Ni-Phl]**$^{-}$ in CH_3CN.

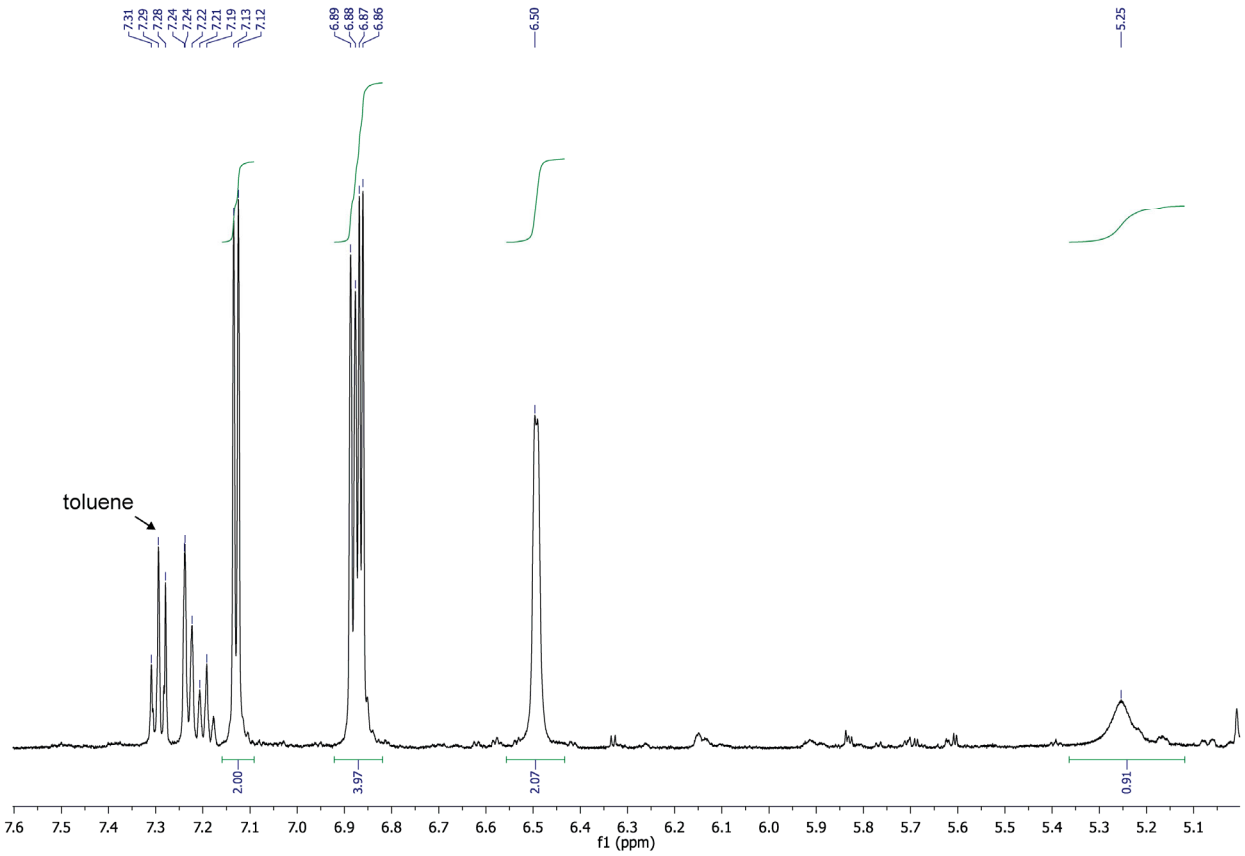

Figure S2. ^{1}H NMR spectrum of **[Ni-Phl]**$^{-}$ in CD_3CN at room temperature.

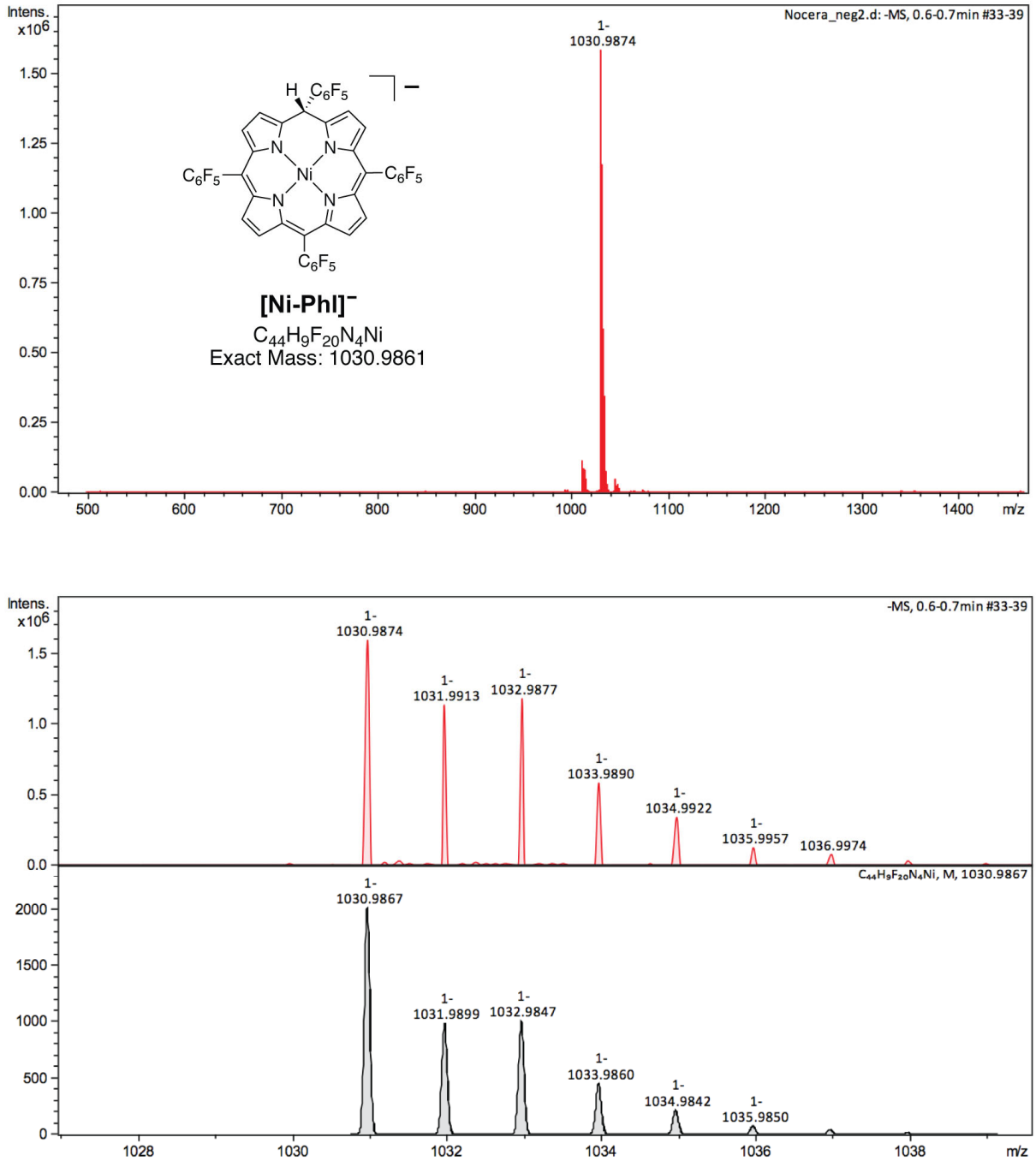

Figure S3. High-resolution MS of **[Ni-Phl]⁻** using negative ion mode.

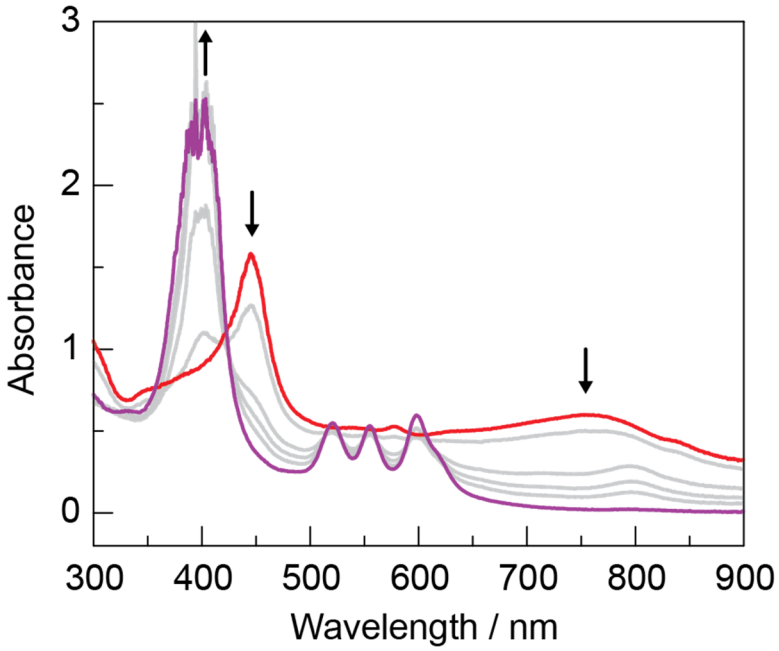

Figure S4. UV-vis absorption spectral change following addition of excess tosic acid to **[Ni-Phl]**$^-$ in CH_3CN. Initial spectrum: —, red; final spectrum: —, purple. Spectra were acquired over a period of 20 s.

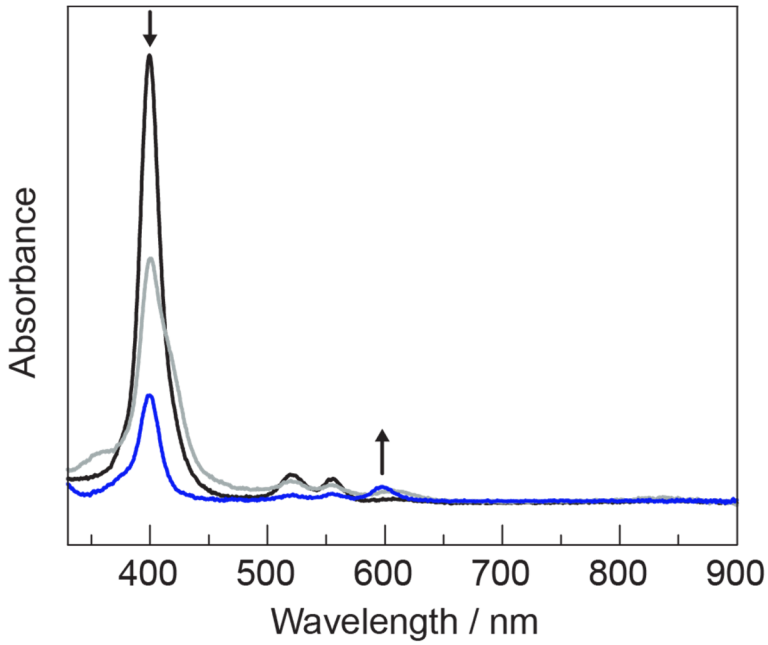

Figure S5. UV-vis absorption spectra of before (—, black) and after (—, blue) 30 min of controlled-potential bulk electrolysis of **Ni-P** at a potential of −1.4 V vs. Fc^{+}/Fc in CH_3CN (0.1 M $TBAPF_6$) in the presence of 4.4 equiv of tosic acid. Working electrode: glassy carbon crucible; counter electrode: platinum wire. The sharp Soret band signal near 400 nm is indicative of a small amount of remaining porphyrin or chlorin signal due to incomplete conversion to **Ni-iBC**.

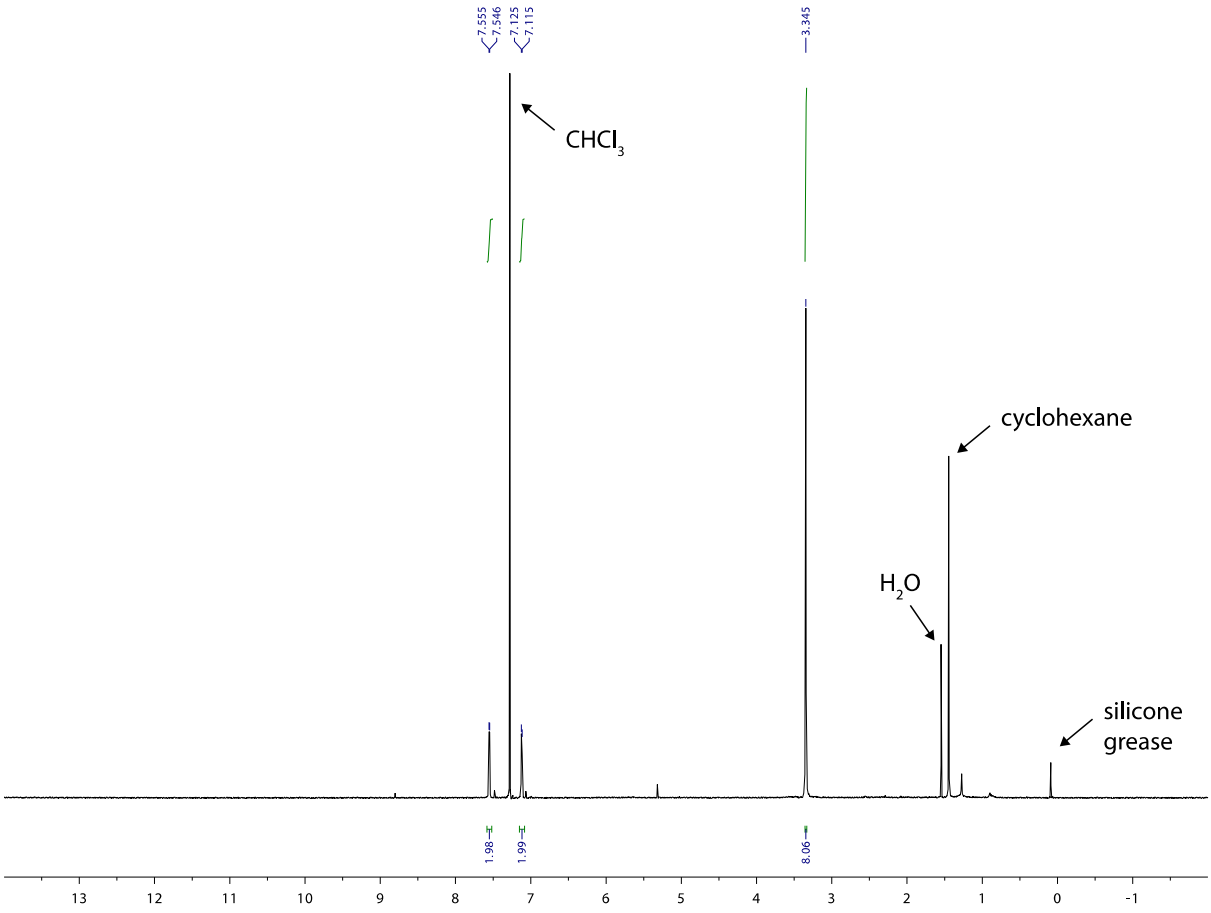

Figure S6. ^{1}H NMR of **Ni-iBC** in $CDCl_3$ at room temperature.

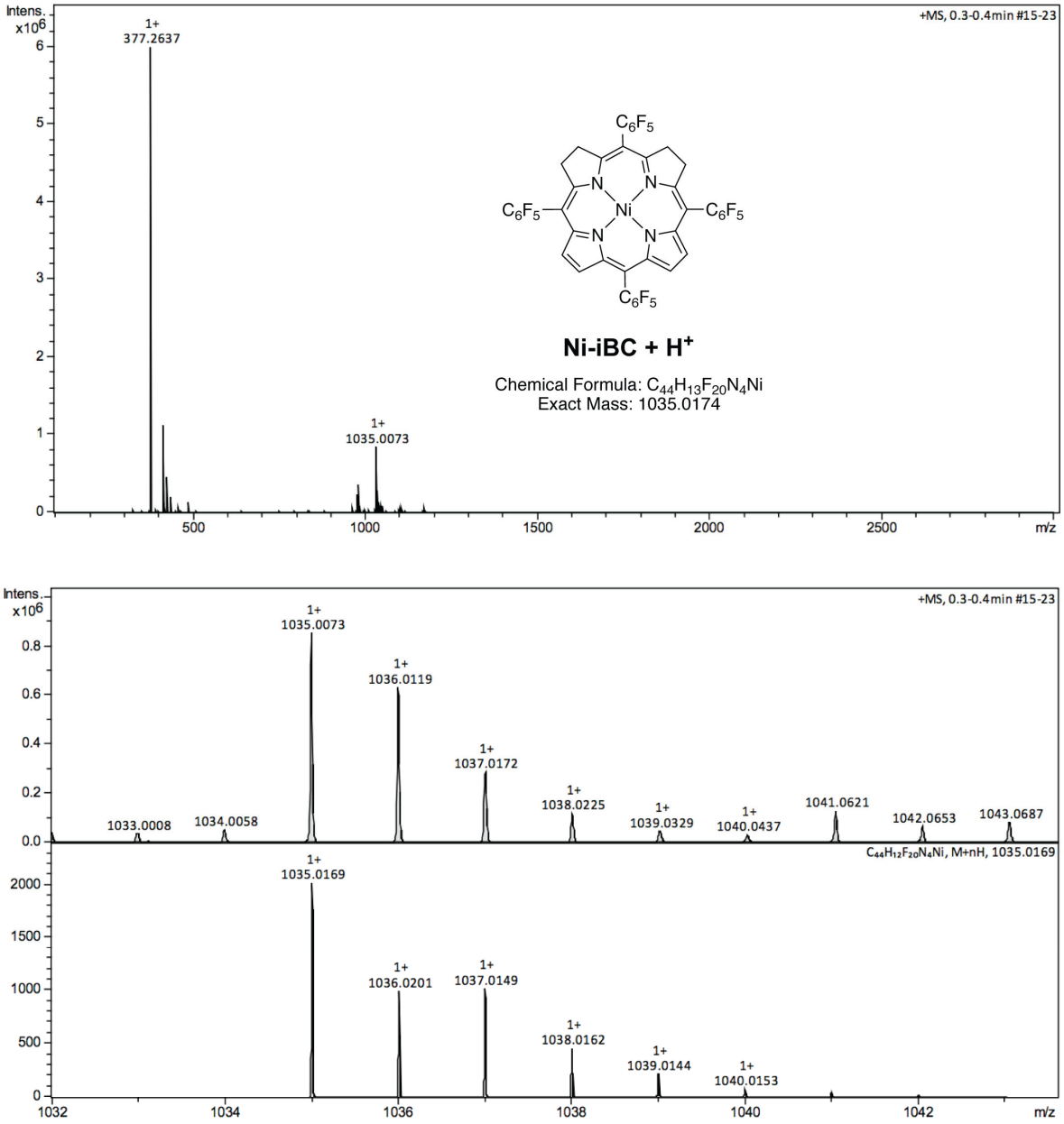

Figure S7. High-resolution MS of **Ni-iBC** using positive ion mode

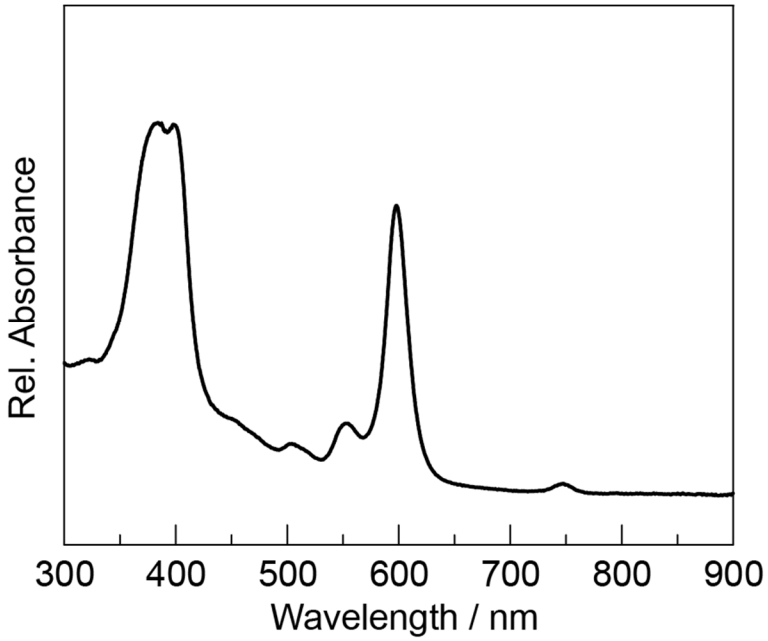

Figure S8. UV-vis absorption spectrum of isolated **Ni-iBC** in CH_3CN following alumina column chromatography.

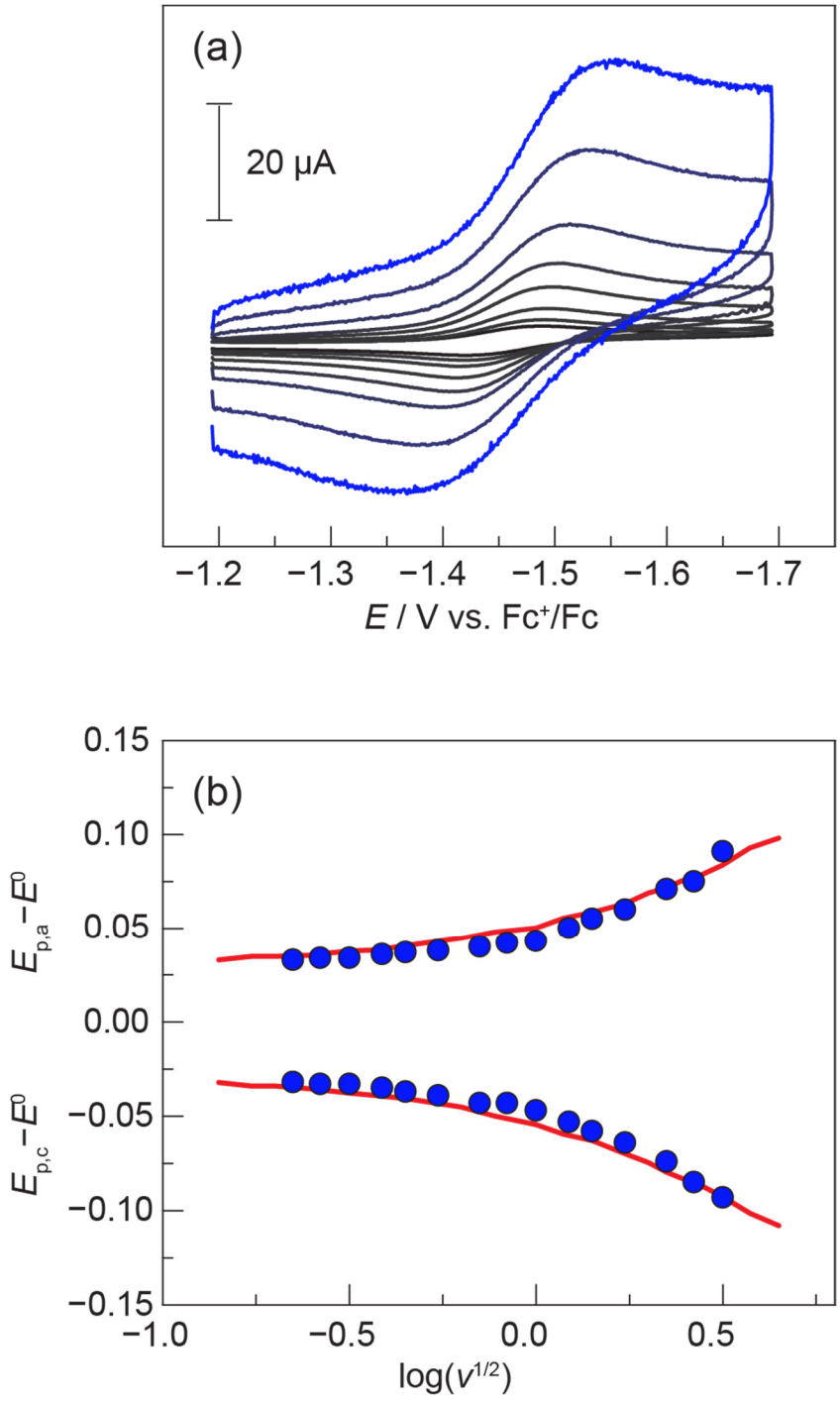

Figure S9. (a) CVs of 0.32 mM **Ni-iBC** in CH_3CN (0.1 M $TBAPF_6$) at scan rates (v) ranging from 0.05 V s^{-1} (—, black) to 10 V s^{-1} (—, blue). (b) Cathodic and anodic peak potential shifts at different scan rates (●, blue dots) along with the working curve (—, red) that furnishes a standard heterogeneous rate constant for electron transfer of k_S^{ap} = 0.014 cm s^{-1}.

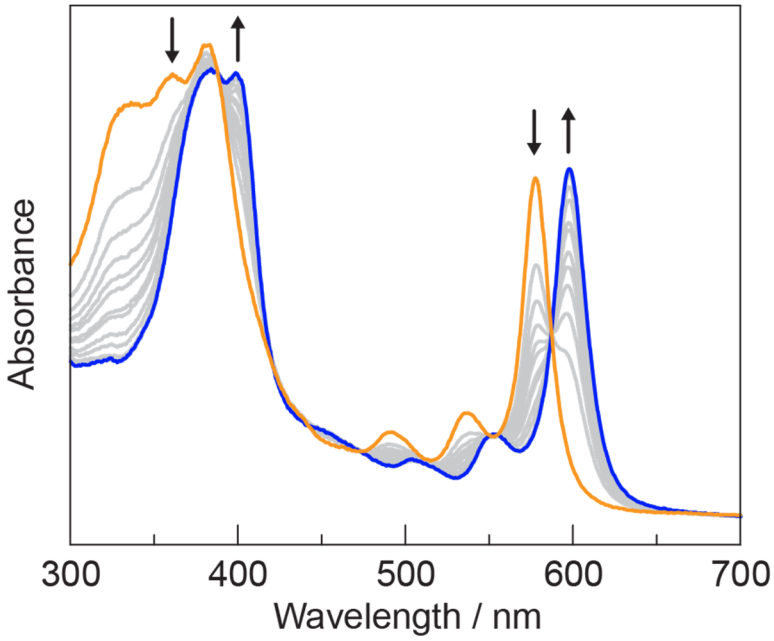

Figure S10. Thin-layer UV-vis spectroelectrochemistry of **Ni-iBC** showing the oxidation of **[Ni-iBC]**$^{-}$ (—, orange) back to **Ni-iBC**^{0} (—, blue). The spectra shown were acquired while the potential was held at −0.1 V vs. Fc^{+}/Fc for 120 s after a potential of −1.6 V vs. Fc^{+}/Fc had been held for 200 s.

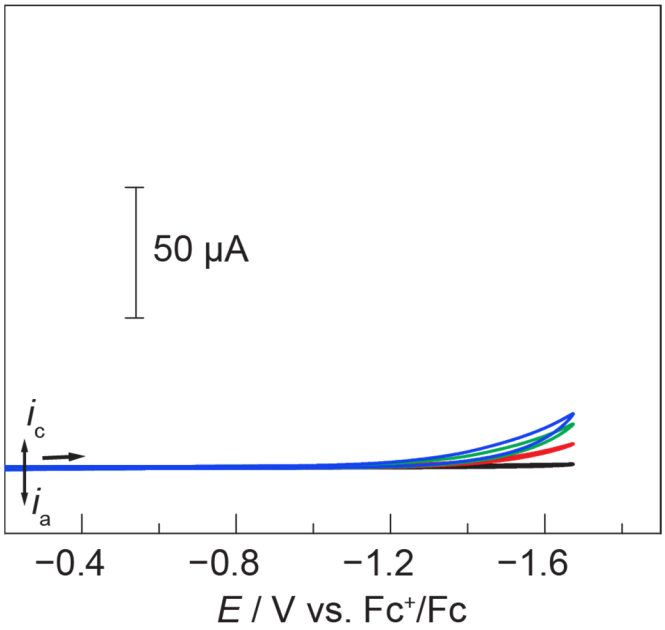

Figure S11. CVs in CH_3CN (0.1 M $TBAPF_6$) at a scan rate of 0.1 V s^{-1} using a glassy carbon working electrode in the presence of only tosic acid at the following concentrations: 0 (—, black), 2.0 (—, red), 5.0 (—, green), and 10.0 mM (—, blue).

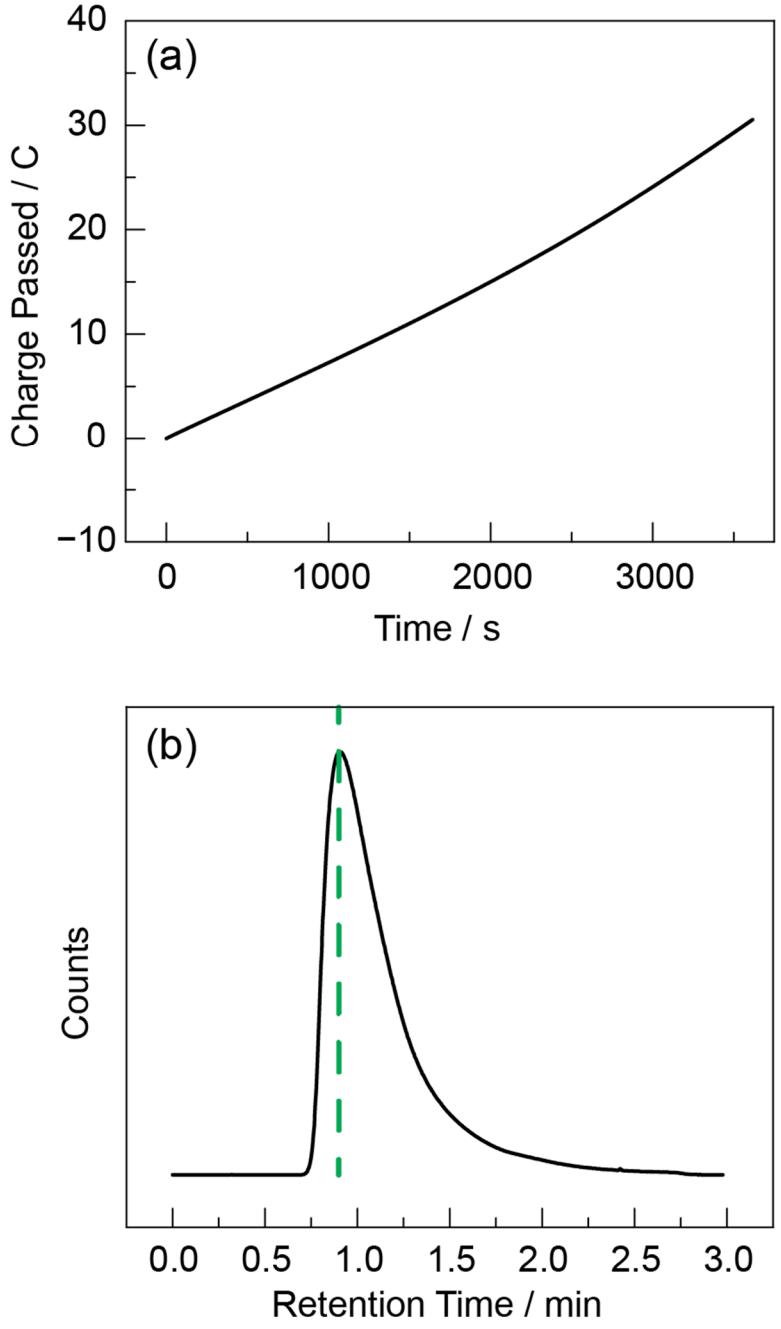

Figure S12. (a) Charge passed during bulk electrolysis of **Ni-iBC** in the presence of 30 mM tosic acid in CH_3CN (0.1 M $TBAPF_6$) at an applied potential of −1.6 V vs. Fc^+/Fc. (b) GC of the headspace following the bulk electrolysis (—, black). The retention time for pure H_2 gas is indicated (– –, dashed green).

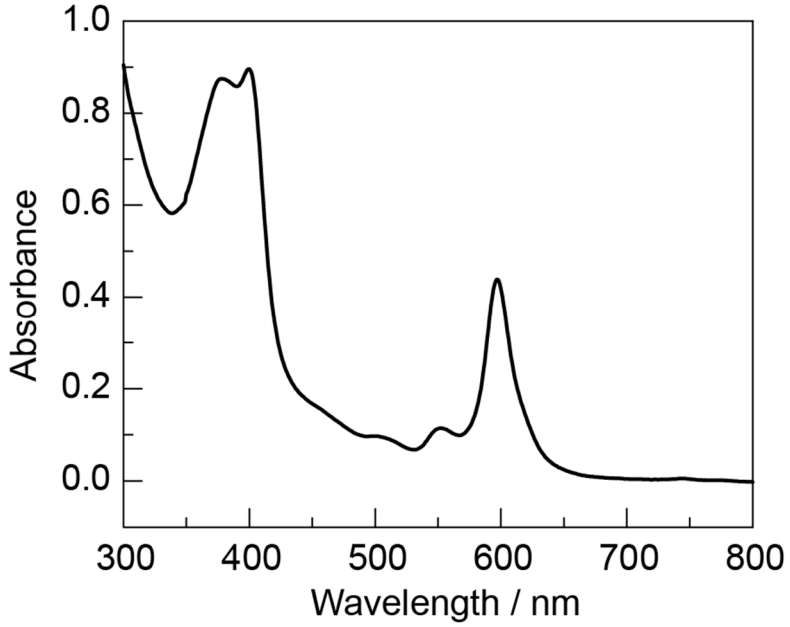

Figure S13. UV-vis absorption spectrum of the resulting solution following bulk electrolysis of **Ni-iBC** in CH_3CN (0.1 M $TBAPF_6$) in the presence of 30 mM tosic acid. The solution was diluted by a factor of 5 in the cuvette used for the absorption spectrum.

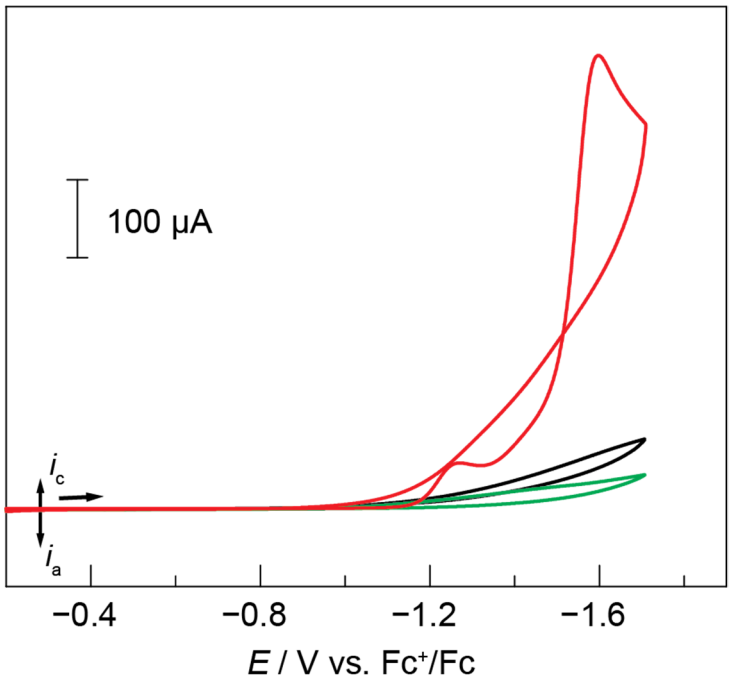

Figure S14. Red trace (—): CV of 0.71 mM **Ni-P** in CH_3CN (0.1 M $TBAPF_6$) at a scan rate of 0.1 V s^{-1} using a glassy carbon working electrode (3.0 mm diameter) in the presence of 50 mM tosic acid. Black trace (—): CV taken using the same working electrode in fresh CH_3CN/electrolyte solution containing only 50 mM tosic acid after a potential of −1.7 V vs. Fc^+/Fc was held in the solution containing 0.71 mM **Ni-P** and 50 mM tosic acid for 2 min. Green trace (—): CV of a freshly polished glassy carbon electrode in the CH_3CN/electrolyte solution containing only 50 mM tosic acid (no **Ni-P** in solution).

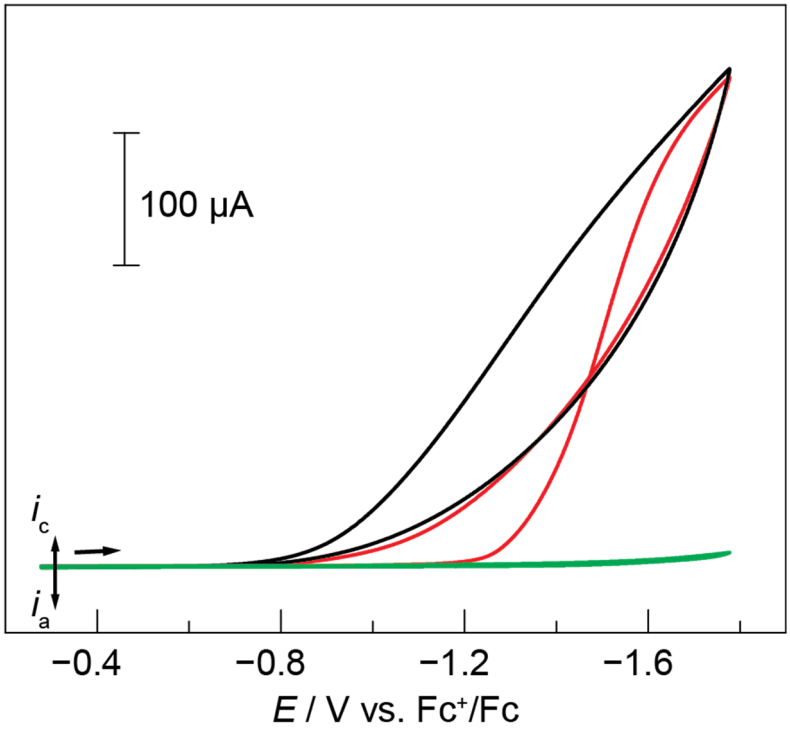

Figure S15. Red trace (—): CV of 1 mM **Ni-iBC** in CH_3CN (0.1 M $TBAPF_6$) at a scan rate of 0.1 V s^{-1} using a glassy carbon working electrode (3.0 mm diameter) in the presence of 50 mM tosic acid. Black trace (—): CV taken using the same working electrode in fresh CH_3CN/electrolyte solution containing only 50 mM tosic acid after a potential of −1.7 V vs. Fc^+/Fc was held in the solution containing 1 mM **Ni-iBC** and 50 mM tosic acid for 2 min. Green trace (—): CV of a freshly polished glassy carbon electrode in the CH_3CN/electrolyte solution containing only 50 mM tosic acid (no **Ni-iBC** in solution).

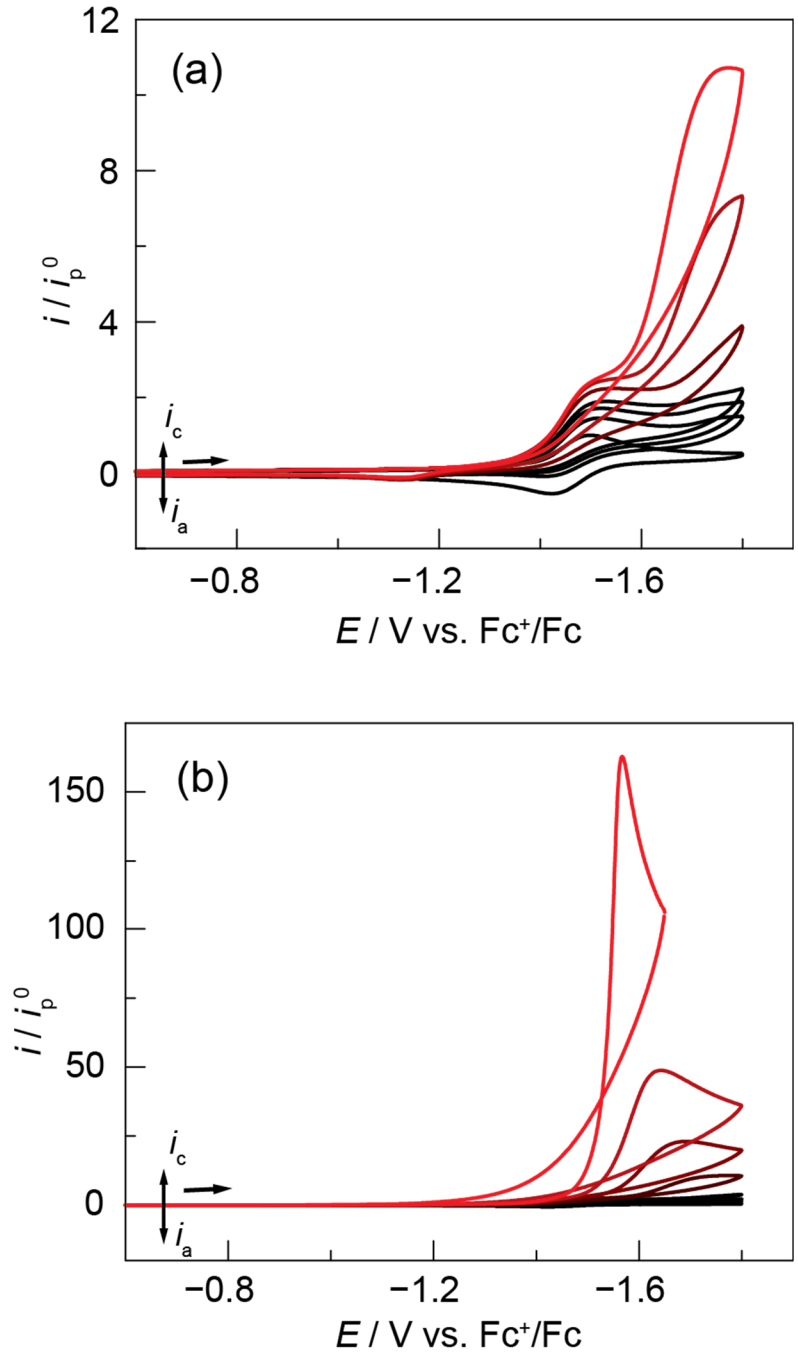

Figure S16. CVs of **Ni-iBC** (0.30 mM) in CH_3CN (0.1 M $TBAPF_6$) at a scan rate of 0.1 V s^{-1} (glassy carbon working electrode) in the presence of trifluoroacetic acid at the following concentrations (from black to red): (a) 0, 0.5, 0.75, 1.0, 2.0, 3.5, and 5.0 mM; (b) 0, 0.5, 1.0, 2.0, 5.0, 10.0, 20.0, and 50.0 mM.

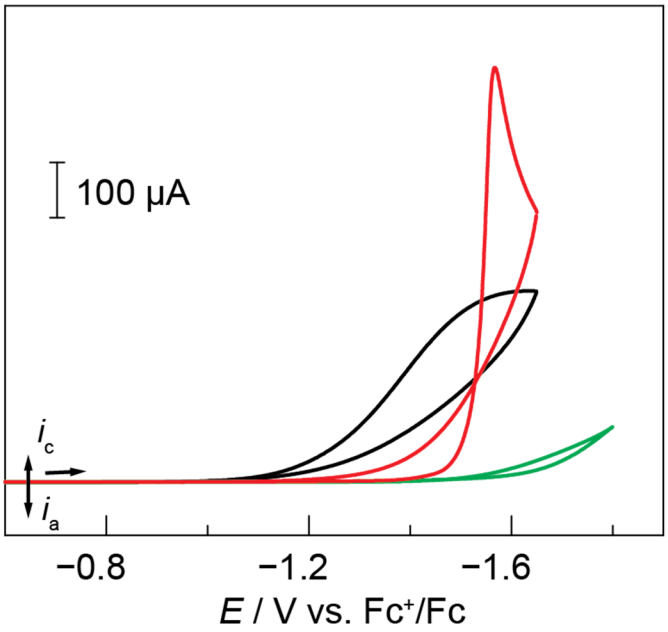

Figure S17. Red trace (—): CV of 0.30 mM **Ni-iBC** in CH_3CN (0.1 M $TBAPF_6$) at a scan rate of 0.1 V s^{-1} using a glassy carbon working electrode (3.0 mm diameter) in the presence of 50 mM trifluoroacetic acid. Black trace (—): CV taken using the same working electrode in fresh CH_3CN/electrolyte solution containing only 50 mM trifluoroacetic acid after a potential of −1.7 V vs. Fc^+/Fc was held in the solution containing 0.30 mM **Ni-iBC** and 50 mM trifluoroacetic acid for 2 min. Green trace (—): CV of a freshly polished glassy carbon electrode in the CH_3CN/electrolyte solution containing only 50 mM tosic acid (no **Ni-iBC** in solution).

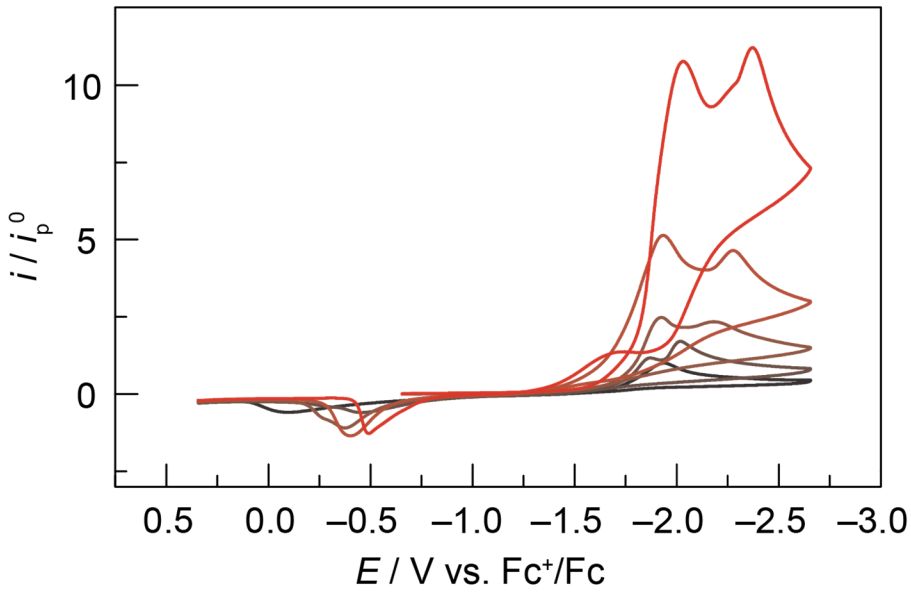

Figure S18. CVs of $Ni(ClO_4)_2 \cdot 6H_2O$ (0.5 mM) in CH_3CN (0.1 M $TBAPF_6$) at a scan rate of 0.1 V s^{-1} (glassy carbon working electrode) in the presence of tosic acid at the following concentrations (from black to red): 0, 1.0, 5.0, 10.0, and 20.0 mM.

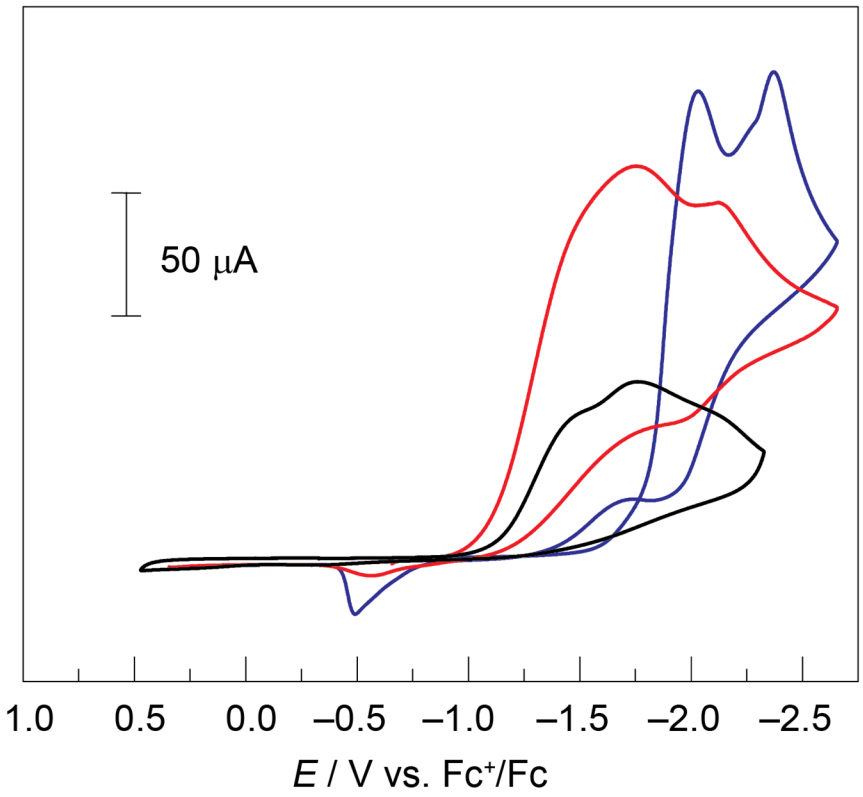

Figure S19. Blue trace (—): CV of 0.5 mM $Ni(ClO_4)_2 \cdot 6H_2O$ in CH_3CN (0.1 M $TBAPF_6$) at a scan rate of 0.1 V s^{-1} using a glassy carbon working electrode (3.0 mm diameter) in the presence of 20 mM tosic acid. Red trace (—): CV taken using the same working electrode in fresh CH_3CN/electrolyte solution containing only 20 mM tosic acid after a potential of −1.7 V vs. Fc^+/Fc was held in the solution containing 0.5 mM $Ni(ClO_4)_2 \cdot 6H_2O$ and 20 mM tosic acid for 3 min. Black trace (—): CV of a freshly polished glassy carbon electrode in the CH_3CN/electrolyte solution containing only 20 mM tosic acid (no $Ni(ClO_4)_2 \cdot 6H_2O$ in solution).

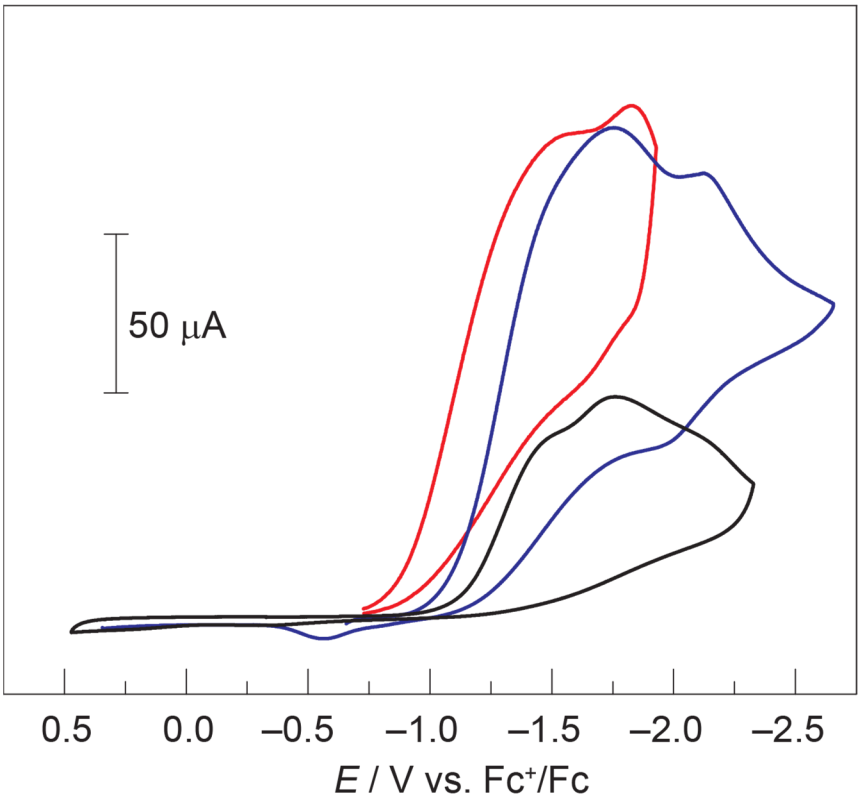

Figure S20. Blue trace (—): CV taken using the same working electrode in fresh CH_3CN/electrolyte solution containing only 20 mM tosic acid after a potential of −1.7 V vs. Fc^+/Fc was held in the solution containing 0.5 mM $Ni(ClO_4)_2{\cdot}6H_2O$ and 20 mM tosic acid for 3 mi. Red trace (—): CV taken using the same working electrode in fresh CH_3CN/electrolyte solution containing only 20 mM tosic acid after a potential of −1.7 V vs. Fc^+/Fc was held in the solution containing 0.5 mM **Ni-iBC** and 20 mM tosic acid for 3 min. Black trace (—): CV of a freshly polished glassy carbon electrode in the CH_3CN/electrolyte solution containing only 20 mM tosic acid.

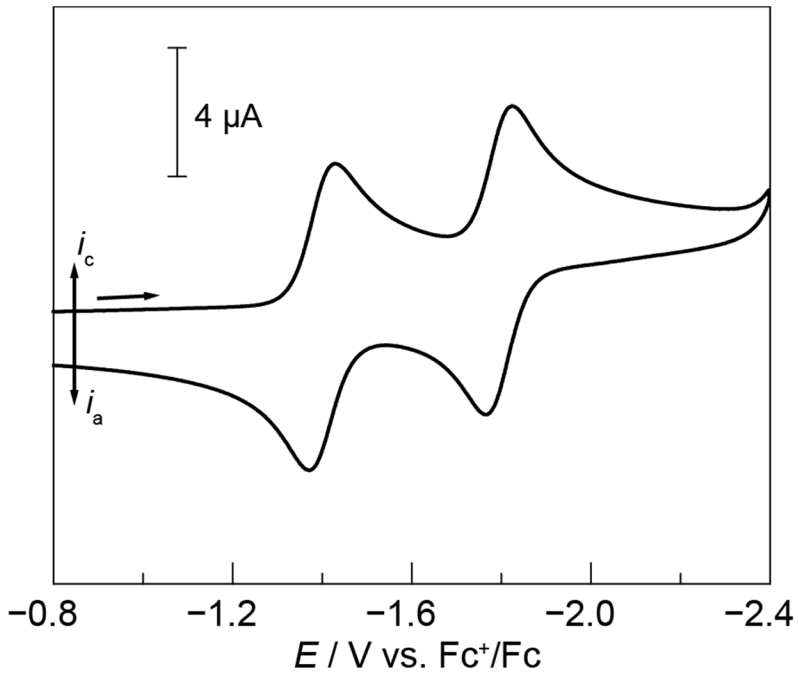

Figure S21. CV of **Zn-P** in CH_3CN (0.1 M $TBAPF_6$) at a scan rate of 0.1 V s^{-1}.